Glacial Isostatic Adjustment modelling of the mid-Holocene sea-level highstand of Singapore and Southeast Asia

Tanghua Li[1*], Stephen Chua[1,a], Fangyi Tan[1,2,a], Nicole S. Khan[3], Timothy Shaw[1], Jędrzej Majewski[1], Aron Meltzner[1,3], Adam Switzer[1,3], Patrick Wu[4], and Benjamin P. Horton[1,3]

[1]Earth Observatory of Singapore, Nanyang Technological University, Singapore, Singapore

[2]Asian School of the Environment, Nanyang Technological University, Singapore, Singapore

[3]Department of Earth Sciences and the Swire Institute of Marine Science, University of Hong Kong, Hong Kong, China

[4]Department of Geoscience, University of Calgary, Calgary, Alberta, Canada

[a] The authors contributed equally

*Corresponding author: Tanghua Li (li.tanghua@ntu.edu.sg)

Key Points:

- We investigate the sensitivity of mid-Holocene sea-level highstand to ice and Earth model parameters of Glacial Isostatic Adjustment models.
- Earth model variation only affects the magnitude unless extraordinarily low upper mantle viscosity is used, while ice model variation changes both the timing and magnitude of the mid-Holocene highstand.
- The highstand along the coasts of inner Sundaland, including west and east coasts of Malay-Thai Peninsula, east coast of Sumatra, and west coast of Borneo, are sensitive to upper (1D) and lower (both 1D and 3D) mantle viscosities.
- The coastlines that are very likely (90% probability) to have the mid-Holocene highstand preservation are northern east coast and central west coast of Malay-Thai Peninsula, east coast of Sumatra, north coast of Java, and southwest coast of Borneo.

Abstract

The mid-Holocene sea-level highstand refers to the development of higher-than-present relative sea levels (RSLs) in far-field regions between 7,000 and 4,000 years ago because of equatorial ocean syphoning and continental levering. The timing, magnitude and spatial variability of the highstand are uncertain and the highstand parameterization in Glacial Isostatic Adjustment (GIA) modelling is understudied. Here, we use the RSL records of Southeast Asia to investigate the sensitivity of the mid-Holocene highstand properties to ice and Earth model parameters, including lithospheric thickness, mantle viscosity (both 1D and 3D), and deglaciation history of Antarctica and global ice sheets. We found that the Earth model variation only affects the magnitude of the mid-Holocene highstand unless low upper mantle viscosity is used. The timing of the highstand moves towards present and there is an absence of the highstand if upper mantle viscosity is $<4.0 \times 10^{19}$ Pa s or $\leq 1.0 \times 10^{19}$ Pa s, respectively. Ice model variation changes both the timing and magnitude of the mid-Holocene highstand. Delaying the ice-equivalent sea level will shift the timing of the highstand later and result in a lower highstand magnitude. We produced a mid-Holocene highstand "treasure map" that considers topography change and accommodation space to guide future RSL data collection efforts in Southeast Asia. The highstand "treasure map" indicates the northern east coast and central west coast of Malay-Thai Peninsula, east coast of Sumatra, north coast of Java, and southwest coast of Borneo are very likely (90% probability) to preserve mid-Holocene RSL data.

1 Introduction

The mid-Holocene highstand is a phenomenon where regions distal from polar ice sheets experienced relative sea levels (RSLs) higher than present-day levels between 7,000 and 4,000 years ago (e.g., Woodroffe and Horton; 2005; Dutton et al., 2015; Kidson, 1982; Mitrovica & Milne, 2002). Mid-Holocene highstands of up to 5 m above present levels have been recorded globally in the Arabian-Persian Gulf (e.g., Al-Mikhlafi et al., 2021; Lokier et al., 2015; Mauz et al., 2022), South America (e.g., Angulo et al., 2006; Fontes et al., 2017; Milne et al., 2005), the Mediterranean (e.g., Mauz et al., 2015; Pirazzoli, 2005) as well as Japan (e.g., Yamano et al., 2019; Yokoyama et al., 2012). However, many of these regions experience significant tectonic deformation that generates additional vertical uncertainties (e.g., Yousefi et al., 2018).

The uncertainty of mid-Holocene highstands (e.g., Chua et al., 2021; Geyh et al., 1979; Horton et al., 2005; Mann et al., 2019; Tan et al., 2023) highlights the need to reconstruct RSL in tectonically stable regions such as Southeast Asia. Except for places near the plate boundaries, Southeast Asia is considered tectonically stable, especially for countries within the Sundaland Core (Hall & Morley, 2004). However the region has spatially and temporally sparse Holocene sea-level data (e.g., Horton et al., 2005; Somboon & Thiramongkol, 1992; Tjia, 1996). Understanding the variability in the timing and magnitude of the mid-Holocene highstand is important for improving Glacial Isostatic Adjustment (GIA) models by constraining the ice and Earth models.

The mid-Holocene sea-level highstand is caused by two mechanisms that cause a fall in RSL in far-field regions (Fig. 1): (1) equatorial ocean syphoning; and (2) continental levering (Mitrovica & Milne, 2002; Mitrovica & Peltier, 1991; Nakada & Lambeck, 1989). Equatorial ocean syphoning describes the migration of water from far-field regions into areas vacated by forebulge collapse and subsidence at the periphery of deglaciation centers to maintain dynamic equilibrium (e.g., Clark et al., 1978; Mitrovica & Peltier, 1991). Continental levering links to vertical land motion of continental margins due to the increasing ocean loading caused by rising sea levels, which induces a subsidence of offshore regions and an uplift of onshore regions (e.g., Lambeck & Nakada, 1990; Mitrovica & Milne, 2002; Nakada & Lambeck, 1989; Walcott, 1972). Numerical solutions employed to reveal and understand the mid-Holocene sea-level highstand began in the 1970s (e.g., Clark et al., 1978; Lambeck et al., 2003; Mitrovica & Peltier, 1991; Peltier et al., 2022; Walcott, 1972; Yokoyama & Purcell, 2021), but fewer studies have exclusively focused on the mid-Holocene sea-level highstand parameterization in GIA models and improvement of the fit with data (e.g., Bradley et al., 2016; Lambeck, 2002; Mitrovica & Milne, 2002; Yokoyama et al., 2012).

Here, we investigate the sensitivity of the mid-Holocene highstand timing, magnitude and spatial variability to ice and Earth model parameters, including lithospheric thickness, mantle viscosity (both 1D and 3D), and deglaciation history of Antarctica only and globally. We compare GIA model predictions from two different ice models ICE-6G_C (Argus et al., 2014; Peltier et al., 2015) and ANU-ICE (e.g., Lambeck et al., 2010, 2014, 2017) with a standardized RSL database from Singapore (Chua et al., 2021). The database has a near-complete Holocene record with more than 130 index points that span from ~9.5 ka BP to present. We identify regions that are sensitive to certain parameters and regions with highstand sensitivity larger than certain thresholds (Steffen et al., 2014), such as 1.25 m, which is larger than the average vertical uncertainty of mid-Holocene RSL data in Southeast Asia (Chua et al., 2021). To guide future RSL data collection efforts in Southeast Asia, we produce a mid-Holocene highstand "treasure map" that considers topography change and accommodation space to highlight locations of highstand records preservation (e.g., Steffen et al., 2014). We validate the highstand "treasure map" with the published records of the highstand from the Southeast Asian region and compare the peak highstand data with peak GIA highstand predictions.

2 Methods

2.1 Glacial Isostatic adjustment models

The GIA models were computed using the Coupled Laplace-Finite Element (CLFE) method (Wu, 2004) with 0.5 × 0.5-degree horizontal resolution near the surface, decreasing with depth to 2.0 × 2.0-degree in the lower mantle to reduce computational resources (Li & Wu, 2019). The model has a temporal resolution of 0.5 ka during the Holocene period (since 12 ka BP) and 1 ka from the Last Glacial Maximum (LGM, 26 ka BP) to 12 ka BP. The GIA models include both the effects of rotational feedback and time-dependent coastlines in the computation of the sea-level equation (Peltier, 1994). The details of the GIA model are described in Li et al. (2022).

We take the ICE-6G_C (VM5a) (Argus et al., 2014; Peltier et al., 2015) as the reference model (Fig. 2, 3). The sensitivity of RSL ($RSL_{Sen}(\theta, \lambda, t)$) to a specific parameter in a GIA model was obtained from the difference between the RSL predictions of the reference model

($RSL_{Ref}(\theta, \lambda, t)$) and a GIA model ($RSL_{Test}(\theta, \lambda, t)$) that allows only one parameter to vary at a time (Fig 2, 4; Steffen et al., 2014; Wu, 2006), as shown in Equation 1.

$$RSL_{Sen}(\theta, \lambda, t) = RSL_{Test}(\theta, \lambda, t) - RSL_{Ref}(\theta, \lambda, t) \quad (1)$$

Here, θ, λ, and t represent latitude, longitude and time, respectively. For simplicity, we may also use $RSL_{Sen}(t) = RSL_{Test}(t) - RSL_{Ref}(t)$ if we do not refer to any specific location. We investigate the Earth model parameters of lithospheric thickness, 1D and 3D viscosity structures in the upper and lower mantle and ice model parameters of global and Antarctic ice-equivalent sea levels (IESLs).

We test a wide range of Earth parameters that were previously used in GIA modelling studies for the region (e.g., Bradley et al., 2016; Lambeck et al., 2014), including lithospheric thickness varying from 30 to 200 km, 1D upper mantle viscosity varying from 1.0 $\times 10^{19}$ to 3.0 $\times 10^{21}$ Pa s, and 1D lower mantle viscosity varying from 1.0 $\times 10^{21}$ to 1.0 $\times 10^{24}$ Pa s. Bradley et al. (2016) suggested that lateral viscosity variations need to be included in the region (e.g., Li et al., 2018; Powell et al., 2021). Therefore, we test the 3D viscosity structures in the upper and lower mantle that were derived from the TX2011 global seismic tomography model (Grand, 2002).

Chua et al. (2021) compared GIA predictions of ICE-6G_C with Holocene RSL data from Southeast Asia. They implied that more ice should melt later than represented in ICE-6G_C during mid-late Holocene, which is likely from Antarctica (Bradley et al., 2016; Tam et al., 2018; Xiong et al., 2020; Yu et al., 2023; Zhang et al., 2021). We therefore test models with 1 ka delay of global and Antarctic IESLs.

To test whether the choice of the ice model changes our results significantly, we also conduct sensitivity tests with the ANU-ICE (e.g., Lambeck et al., 2010, 2014, 2017) as the reference ice model while using the same Earth models.

2.2 Mid-Holocene highstand databases for Singapore and Southeast Asia

We take Singapore as a sample site to study the changes in the pattern of RSL predictions and magnitude and timing of the highstand (i.e., maximum positive RSL reached during the Holocene) with the variation of Earth and ice parameters, and how the changes affect the fit with the proxy RSL data. Singapore has numerous quality-controlled RSL data during the Holocene, although a temporal gap does exist during the mid-late Holocene (Fig. 2; Chua et al., 2021).

We compiled a mid-Holocene peak highstand database for Southeast Asia (e.g., Geyh et al., 1979; Mann et al., 2023; Meltzner et al., 2017; Somboon & Thiramongkol, 1992; Zhang et al., 2021). We re-evaluated published mid-Holocene (7 – 4 ka) RSL data following the methodology of the HOLocene SEA-level variability (HOLSEA) working group (Khan et al., 2019). We produced sea-level index points (SLIPs) from sedimentary indicators (e.g., mangrove sediments) and fixed biological indicators (e.g., coral microatolls, oyster belts) that occupy constrained vertical ranges with respect to the tides. A SLIP represents the RSL position at a given point in time, with both temporal and vertical uncertainty (Shennan et al., 2015). To produce a SLIP the indicative meaning of the sea-level indicator must be established. The indicative meaning (Table S1 and S2) comprises an indicative range (IR), which is the vertical range of the proxy's relationship with tide levels, and a reference water level (RWL), or central tendency of the indicative range (Horton et al., 2000; Ian Shennan, 1986; Van de Plassche, 1986). Sea-level indicators with less constrained indicative ranges were used to produce marine (e.g., massive corals, calcareous algal crust, eroded coral microatolls) and terrestrial (e.g., beach ridges) limiting data, which indicate a minimum and maximum bound on RSL respectively (Shennan et al., 2015).

To calculate RSL, we subtracted the RWL from the sample elevation, both of which are in the same datum (Shennan and Horton, 2002). All sources of vertical uncertainty associated with determining the elevation of the sample (e.g., levelling uncertainty, tidal uncertainty) were added in quadrature with the uncertainty in defining the sample's indicative meaning (e.g., the IR uncertainty, which is half the IR) to derive the total RSL uncertainty (Shennan & Horton, 2002). For coral microatoll samples whose elevations were reported relative to the elevations of living counterparts (Majewski et al., 2018; Meltzner et al., 2017), the sample elevations as the elevations are themselves estimates of RSL (Tan et al., 2023).

We calibrated all radiocarbon dates in OxCal 4.4 (Ramsey, 2001) using the latest calibration curves, IntCal20 (Reimer et al., 2020) and Marine20 (Heaton et al., 2020). We obtained the marine reservoir correction (ΔR) by selecting the nearest data source from the marine20 ΔR database (Reimer & Reimer, 2001), except for data from Meltzner et al. (2017) (supplementary text). All U-Th dates in this database were based on the decay constants of Cheng et al. (2013).

We assigned quality ranking to all data points based on the susceptibility of the samples to age and/or elevation errors (Tan et al., 2023). The mid-Holocene peak highstand database is summarised in Table 1 with full citations of the published studies.

2.3 Treasure map of the mid-Holocene highstand data

To guide future mid-Holocene RSL data collection, we produce a mid-Holocene highstand "treasure map" that identifies regions that are likely (67% probability) and very likely (90% probability) to have highstand record preservation. We calculate the mean and standard deviation of RSL predictions from the GIA model ensemble consisting of 45 1D models and 2 3D models using the same ice model (e.g., ICE-6G_C; Fig. 5). Assuming the highstand prediction uncertainties are normally distributed with the mean and standard deviation as calculated from the GIA model ensemble, we estimate the probability distribution of having a highstand during the Holocene period in the region.

The "treasure map" considers the residual between present-day topography ($T_p(\theta,\lambda)$) and accommodation space produced by the predicted highstand elevations (i.e., paleotopography) across Southeast Asia. We identify the regions ($R(\theta,\lambda,t)$) that potentially have highstand record preservation at time t, which were previously below sea level ($T(\theta,\lambda,t) \leq 0$) but now sit above present-day sea level ($T_p(\theta,\lambda) > 0$) as shown in Equation 2.

$$R(\theta,\lambda,t) = \begin{cases} T(\theta,\lambda,t) \leq 0 \\ T_p(\theta,\lambda) > 0 \end{cases} \quad (2)$$

$T_p(\theta,\lambda)$ is the present-day topography from the GEBCO_2022 Grid (Ioc, 2003), which is on a 15 arc-second interval grid. $T(\theta,\lambda,t)$ is the paleotopography at time t, which is generated following Peltier (2004):

$$T(\theta,\lambda,t) = RSL(\theta,\lambda,t) + \left[T_p(\theta,\lambda) - RSL\left(\theta,\lambda,t_p\right)\right] \quad (3)$$

where $RSL\left(\theta,\lambda,t_p\right)$ and $RSL(\theta,\lambda,t)$ are the present-day sea level and sea level at time t, respectively. We combine the $R(\theta,\lambda,t)$ through the whole Holocene period to define $R(\theta,\lambda)$, which is the total area with potential to preserve evidence of the mid-Holocene highstand (Fig. 6).

We validate the highstand "treasure map" against the mid-Holocene peak highstand database for Southeast Asia (Table 1) by projecting the peak highstand data locations on the "treasure map" to confirm the presence of the mid-Holocene highstand preservation in the region (Fig. 6). We also compare the peak highstand data with the peak GIA highstand predictions (Fig. 7). Although the timing of compiled peak highstand data might be different from that of peak GIA highstand predictions (e.g., 6.5 ka BP with ICE-6G_C), the magnitude of the highstand should be no lower than (i.e., equal or higher than) the amplitude of the peak highstand data in Table

1 and comparison with peak GIA highstand predictions can validate the GIA model performance.

3. Comparison of GIA model predictions with RSL data from Singapore

The RSLs predicted by the ICE-6G_C (VM5a) reference model are consistently higher than early Holocene (12-8 ka BP) RSL data in Singapore, although the misfit magnitude decreases from ~15 m at 9.5 ka BP to ~5 m at 8 ka BP and intersects with the RSL data at ~6 ka BP (Fig. 2A). The model predicted highstand peaks at 6.5 ka BP with a magnitude of 3.6 m while the RSL data shows the peak highstand should be ~6 ka BP or later with a magnitude of ~3.9 ± 1.1 m or higher. Following the highstand, the predicted RSL declines nearly linearly to present level (0 m) while RSL data shows lower-than-present sea level between 2.5 and 1 ka BP.

3.1. Sensitivity of the mid-Holocene highstand in Singapore to Earth and ice model parameters

Decreasing the upper mantle viscosity from 5.0×10^{20} Pa s to 1.0×10^{20} Pa s (e.g., Bradley et al., 2016; Lambeck et al., 2014) lowers the RSL prediction by ~2.5 m during the early-mid Holocene and the peak highstand decreases by 64% from 3.6 m to 1.3 m at 6.5 ka BP (Fig. 2A). Increasing the lower mantle viscosity from ~2.8×10^{21} Pa s (average lower mantle viscosity of VM5a) to 2.0×10^{22} Pa s (Horton et al., 2005; Lambeck et al., 2014) raises the RSL prediction by ~1.5 m during the early-mid Holocene and the peak highstand increases by 44% from 3.6 m to 5.2 m at 6.5 ka BP.

Incorporating 3D upper mantle viscosity lowers the prediction by ~1 m in the early Holocene and intersects with the prediction of ICE-6G_C (VM5a) at 8 ka BP, while the peak highstand increases slightly by 8% to 3.9 m at 6.5 ka BP. Incorporating 3D lower mantle viscosity has a similar effect to increasing the lower mantle viscosity to 2.0×10^{22} Pa s and both models intersect at 7 ka. However, the prediction for the model incorporating 3D lower mantle viscosity is slightly higher by ~0.5 m in early-mid Holocene and lower by ~0.3 m during mid-late Holocene. In all the above instances, changing the Earth model parameters only affects the magnitude of the highstand and does not influence the timing of the highstand.

The highstand magnitude is insensitive to the lithospheric thickness variation (Fig. 2B). Although a thicker lithosphere produces a smaller magnitude of lithospheric flexure and continental levering (Kaufmann et al., 1997; Mitrovica & Milne, 2002; Nakada & Lambeck, 1989), it also produces broader forebulge subsidence that accommodates more water migrating from far-field regions, and the two mechanisms (i.e., equatorial ocean syphoning and continental levering, Fig. 1) contribute comparably in magnitude but opposite in direction to the far-field RSL changes (Mitrovica & Milne, 2002).

With the increase of upper mantle viscosity, the peak highstand magnitude increases significantly and reaches the maximum of 4.4 m with viscosity of 2.0×10^{21} Pa s before decreasing (Fig. 2C). We notice a shift in the timing of the peak highstand from 6.5 ka BP towards present when upper mantle viscosity is $< 4.0 \times 10^{19}$ Pa s, and an absence of the highstand when upper mantle viscosity is $\leq 1.0 \times 10^{19}$ Pa s. The latter is because exceptionally low viscosity leads to much faster relaxation, with equilibrium reached by the mid-Holocene, so no deformation exists during the mid-late Holocene to cause the highstand. With an increase of the lower mantle viscosity, the peak highstand increases notably and reaches the maximum of 5.2 m with viscosity of 2.0×10^{22} Pa s and then decreases gradually to 4.8 m with viscosity of 1.0×10^{24} Pa s (Fig. 2D).

Delay of the global IESL by 1 ka lowers the prediction by ~8 m at 10 ka BP (Fig. 2A). The difference with ICE-6G_C (VM5a) decreases towards the peak highstand, whose timing is shifted by 1 ka from 6.5 ka BP to 5.5 ka BP, with magnitude decreasing by 11% to 3.2 m. Similarly, delay of the Antarctic IESL by 1 ka shifts timing of the peak highstand to 5.5 ka BP with magnitude decreasing by 25% to 2.7 m. Here, the early Holocene RSL prediction only lowers by ~1 m compared to the ICE-6G_C (VM5a) reference model and the difference increases to ~2 m at 7.5 ka BP, during which the discrepancy between the global IESL (ICE-6G_C) and that with a 1ka delay in the Antarctic component (ICE-6G_C with Antarctica IESL 1 ka delay) is largest (Fig. S1). Unlike changing Earth model parameters, variation of the IESL affects both the magnitude and timing of the highstand.

We infer that for the early-mid Holocene, a decrease of the upper mantle viscosity and delay of IESL improve the model fit with RSL data, while an increase of lower mantle viscosity and incorporation of 3D viscosity in the lower mantle enlarge the misfit. This suggests that the RSL data from Southeast Asia prefer lower viscosities in the upper mantle and later ceasing of melting from Antarctica than represented in the ICE-6G_C model (Bradley et al., 2016; Lambeck et al., 2014; Zhang et al., 2021). The sensitivity patterns of the highstand magnitude to upper and lower mantle viscosity variations (Fig. 2C & D) indicate the importance of considering the Earth model uncertainties (Li et al., 2020; Melini & Spada, 2019) and the non-uniqueness of using highstand information to constrain the mid-late Holocene melting histories (Mann et al., 2023; Mitrovica & Peltier, 1991; Nakada & Lambeck, 1989; Nunn & Peltier, 2001; Tan et al., 2023). Because the highstand change due to upper and lower mantle viscosity variation may compensate each other (e.g., a decrease in the upper mantle and an increase in the lower mantle), the confounding effect of the two can further obscure and interact with the melting signal.

4. Mid-Holocene highstand in Southeast Asia

The ICE-6G_C (VM5a) model predicted highstand first emerged along the Malacca Strait, east coast of Sumatra and southwest coast of Borneo at ~8.5 ka BP with magnitude of 0.5-1 m (Fig. S2). The highstand expanded outwards and reached the highest levels (~4.5 m) in Southeast Asia at 6.5 ka BP and decreased afterwards with consistent highstand distribution pattern (Fig. S2). Hereafter, we focus on the highstand distribution pattern at the peak highstand timing of 6.5 ka BP.

At 6.5 ka BP, highstands existed across all regions of Sundaland and the highstand contours follow the coastlines of outer Sundaland (Fig. 3). Negative RSLs (RSLs below present) at 6.5 ka BP are found in the South China Sea and Indian Ocean. The pattern of highstand on land and negative RSLs offshore is consistent with the highstand patterns revealed in Australia (Lambeck, 2002), South America (Milne et al., 2005), and previous analyses in the Malay-Thai Peninsula (Horton et al., 2005). Peak highstand magnitudes of over 4 m are estimated for the southern Malacca Strait and along the east coast of Sumatra. The highstand magnitude decreases westwards and southwards and reaches ~0.5 m or less near the northern tip of Aceh and ~2 m along the south coast of central Java， respectively. The highstand is ~3 m along the coast of Borneo and east coast of Malay-Thai Peninsula, ~3.5 along the northern coasts of the Gulf of Thailand and decreases westwards and eastwards. Note that the consistently higher highstand in the west coast compared to the east coast of Malay-Thai Peninsula matches the reconstructed highstand records of Zhang et al. (2021).

4.1 Sensitivity of the mid-Holocene highstand in Southeast Asia to Earth and ice model parameters

Decreasing the upper mantle viscosity from 5.0×10^{20} Pa s to 1.0×10^{20} Pa s decreases the RSL by > 2 m at 6.5 ka BP around the central Sundaland and the RSL sensitivity decreases outwards going perpendicular to the coastlines and increases to over 2 m in South China Sea (Fig. 4A). The regions with sensitivity ≥ 1.25 m are the coasts of the Gulf of Thailand, Malay-Thai Peninsula, Sumatra (except Aceh), northern Java and Borneo (except northern tip). The RSL sensitivity to an increase in lower mantle viscosity from ~2.8×10^{21} Pa s to 2.0×10^{22} Pa s at

6.5 ka BP is distinct from the sensitivity to a decrease in the upper mantle viscosity (Fig. 4A & B), showing more than 2 m of higher RSL centered along the east coast of the Malay-Thai Peninsula. The region with sensitivity ≥ 1.25 m shrinks towards central Sundaland compared with the region with sensitivity ≥ 1.25 m due to a decrease in the upper mantle viscosity.

Incorporation of 3D viscosity structures in the upper and lower mantle both lead to higher RSL at 6.5 ka BP along the east coast of Malay-Thai Peninsula and central west coast of Borneo but with differing magnitudes: over 0.5 m for incorporation of a 3D upper mantle and over 1.5 m for a 3D lower mantle, respectively (Fig. 4C & D). The RSL sensitivities decrease going outwards. The region with sensitivity ≥1.25 m due to 3D lower mantle (Fig. 4D) further shrinks towards the central Sundaland compared with the sensitivity to 1D lower mantle viscosity increase (Fig. 4B), although the patterns are very similar.

Because the highstand is relatively insensitive to the lithospheric thickness change (Fig. 2B), an increase of the lithospheric thickness from 60 km to 90 km only induce a RSL sensitivity of < 0.5 m in magnitude at 6.5 ka BP with negative sensitivity along the coastlines in Southeast Asia (Fig. S3).

Because shifting the IESL by 1 ka towards the present also shifts the timing of the peak highstand (Fig. 2A) by 1 ka, we compare the RSL predictions at the timing of peak highstand of test models with the reference model ICE-6G_C (VM5a) via $RSL_{Test}(5.5) - RSL_{Ref}(6.5)$ (Fig. 4E & F). RSL peak highstand sensitivities to 1 ka delay of Antarctic and global IESLs show similar pattern of negative sensitivity in the central Sundaland with magnitude of ~1.0 m for the former and of ~0.5 m for the latter and sensitivity increases outwards going perpendicular to the coastlines (Fig. 4E & F). Because only ~50% of the global IESL of ICE-6G_C is from Antarctic component at 6.5 ka BP (Fig. S1), shifting the global IESL produces about half the magnitude of the peak highstand sensitivity produced by shifting the Antarctic IESL.

The patterns of highstand sensitivity to Earth and ice model parameters in Southeast Asia show some similarities especially in the inner Sundaland, making it challenging to constrain certain parameters via the observational highstand data. More sophisticated techniques on separating RSL contributions from different large ice sheets (e.g., sea-level fingerprinting, Lin et al., 2021) and the spatial gradient among a geographical spread of sea-level data (Kendall et al., 2003; Liu et al., 2016) need to be considered in future studies. Additionally, other types of GIA observational data (e.g., GPS data) from the region need to be included in the inversion process to better constrain GIA input parameters (Mitrovica & Forte, 2004; Peltier et al., 2015; Sasgen et al., 2017).

5. "Treasure map" of the mid-Holocene highstand

The pattern of mean RSL determined from the GIA model ensemble at 6.5 ka BP is very similar to the pattern of RSL at 6.5 ka BP of ICE-6G_C (VM5a). The magnitude of the former is only smaller by ~0.5 m than the latter (Fig. 3, 5A), because only one parameter is explored in broad range each time and the rest of the parameters are fixed the same as the reference model ICE-6G_C (VM5a). Peak RSL of ~4 m is located along the southern Malacca Strait and east coast of Sumatra, decreasing to the northeast and southwest and reaching ~-1 m or less in the Indian Ocean and South China Sea (Fig. 5A). The standard deviation of RSL predictions shows similar pattern as the mean RSL at 6.5 ka BP, with much smaller magnitude of ~2 m or less in the inner Sundaland (Fig. 5B).

With the assumption that highstand prediction uncertainties are normally distributed with the mean and standard deviation as calculated from the GIA model ensemble, we identify regions that are likely (67% probability) to have preserved evidence of a mid-Holocene highstand. These areas are concentrated in Bangkok, Mekong River Delta, northern east coast and central west coast of Malay-Thai Peninsula, east coast of Sumatra, north coast of Java, and southwest coast of Borneo (Fig. 6A).

The compiled peak highstand database is summarized in Table 1 (The HOLSEA template spreadsheet is in the supplementary) and overlain on the "treasure map" in Fig. 6A. The locations of data from Thailand (data No. 1, Table 1), southeast Vietnam (data No. 4, 5), east (data No. 7, 8) and west (data No. 9, 10) coasts of Malay-Thai Peninsula, and Singapore (data No. 11) of highstand records from sedimentary materials (purple dots in Fig. 6A) match well with areas showing highstand preservation denoted in the "treasure map". This validates our assumption that sedimentary material requires time and accommodation space to accumulate (e.g., Dura et al., 2016; Kelsey et al., 2015; Törnqvist et al., 2021) in identified locations in the "treasure map". However, the highstand records (data No. 2-3, 6, 12-16, Table 1) derived from corals and oysters (green dots in Fig. 6A) do not match the "treasure map" as well as the sedimentary records because corals and oysters do not necessarily need the accommodation space. Kelsey et al. (2015) reconstructed the sea-level history in Aceh, Sumatra and found no evidence of a mid-Holocene sea-level highstand record, which is consistent with our "treasure map" (blue dot in Fig. 6A).

With the exception of the Chao Phraya Delta (Somboon & Thiramongkol, 1992), all peak highstand data are in agreement with peak GIA highstand predictions within 2σ uncertainties, validating the performance of the GIA models (Fig. 7). Chao Phraya Delta has an exceptionally high RSL of 7.0 $\pm$ 1.3 m, which is much higher than the rest of the highstand records in Southeast Asia (Table 1) and is higher than the predicted highstand magnitude of 3.6 $\pm$ 2.9 m (Fig. 7) and might be due to some unknown local influences.

Note that our “treasure map” does not consider the non-GIA regional and local factors that may affect the preservation and elevation of the highstand records, such as tectonics (e.g., Subarya et al., 2006), subsidence (e.g., Sinsakul, 2000), erosion and deposition (e.g., Anthony et al., 2015), and post-depositional change (e.g., Joyse et al., 2023), which all need to be considered for future sea-level reconstructions. For example, the Mekong River Delta is very likely (90% probability) to have the highstand preservation (Fig. 6B), but no SLIPs for the highstand have been obtained. Sea-level records for the Mekong River Delta have been derived only for the early Holocene (Nguyen et al., 2010; Tjallingii et al., 2010) and the late (4 ka BP - present) Holocene (Stattegger et al., 2013). However, the mid-Holocene highstand is largely inferred (e.g., Li et al., 2012) or estimated using limiting data (e.g., Kahlert et al., 2021; Stattegger et al., 2013) due to the lack of mid-Holocene SLIPs. No Holocene sea-level data points exist above modern sea levels (Tjallingii et al., 2014), likely due to the lowering of the Mekong River Delta region due to sediment compaction (Zoccarato et al., 2018). Sediments are also frequently tidally inundated and eroded due to the highly dynamic depositional environment composed of a dense riverine network characterized by significant lateral sediment bar drifts during the late Holocene (Tamura et al., 2012), and exacerbated by human activities in recent years (Anthony et al., 2015).

Similarly, Bangkok sits on the Chao Phraya Delta and experienced significant subsidence in recent years due to sediment compaction due to urbanization, exacerbated by modern groundwater extraction (Sinsakul, 2000). The west coast of Sumatra also experienced significant land-level change due to tectonic subsidence caused by the Sunda megathrust, where average subsidence rates were 2-14 mm/yr between 1950 and 2000 (Natawidjaja et al., 2007). Thus, any evidence of the highstand may have been removed by coastal processes as the nearshore zone shifts landward due to recent land-level fall.

Although the data from these regions may not be ideal for validating GIA models given the large uncertainties in local vertical land motion, comparison of GIA highstand predictions and proxy RSL records from these regions can reveal the local/regional subsidence signal (e.g., King et al., 2021; Liberatore et al., 2022; Wang et al., 2020). For example, Sefton et al. (2022) reconstructed the RSL history on Pohnpei and Kosrae and revealed a ~4.3 m RSL rise over the past ~5.7 ka BP, while the GIA model shows a RSL fall from an over 2.5 m highstand at ~6 ka BP. The discrepancy indicates a mid-late Holocene subsidence of ~1 mm/yr on the two islands.

The regions that are very likely (90% probability) to have the highstand record preservation follow a similar pattern as the likely regions (67% probability) of highstand preservation but with smaller coverage, including northern east coast and central west coast of Malay-Thai Peninsula, east coast of Sumatra, north coast of Java, and southwest coast of Borneo (Fig. 6). These regions could be the key potential areas for future sea-level data collection efforts.

6 Sensitivity test with the ANU-ICE model

The ANU-ICE (e.g., Lambeck et al., 2010, 2014, 2017) model, coupled with VM5a Earth model, generates a similar peak highstand pattern as ICE-6G_C (Argus et al., 2014; Peltier et al., 2015) ice model (Fig. 3, S4), although the ANU-ICE model produces a later timing of peak highstand by ~0.5 ka (6 ka BP) and of ~1 m lower magnitude (~3.5 m along the Malacca Strait). Because the deglaciation history (i.e., IESL) of ANU-ICE decelerates later and ceases later than that of ICE-6G_C (Fig. S1), this leads to shorter time for the accumulation of the highstand formation when coupled with the same Earth model (Argus et al., 2014; Bradley et al., 2016; Lambeck et al., 2014, 2017; Peltier et al., 2015).

Fixing ANU-ICE as the reference ice model, the RSL sensitivities to upper and lower mantle viscosity changes (both 1D and 3D) and shifts of global and Antarctic IESLs in Singapore and Southeast Asia are generally consistent with the sensitivity results of ICE-6G_C (Fig. 2-6, S4-S8). We observe that the ANU-ICE model provides a better fit with the data from Singapore (Fig. S5A) because the global IESL of ANU-ICE was developed to fit RSL data from far-field regions including Singapore (Bird et al., 2007, 2010; Lambeck et al., 2014), while the global IESL of ICE-6G_C is exclusively tuned to fit the tectonically-corrected RSL records from Barbados (Peltier et al., 2015). We also notice the abnormal predicted RSL curve in Singapore from the model with Antarctic IESL shifted 1 ka towards present (cyan solid line in Fig. S5A), which is dominated by its IESL (blue dotted line in Fig. S1). The Antarctic IESL of ICE-6G_C differs significantly from that of ANU-ICE (Fig. S1). The former Antarctic IESL contribution is ~14 m since the LGM and ~12 m since the start of the Holocene, whereas the latter is ~28 m and ~26 m, respectively (Argus et al., 2014; Lambeck et al., 2014, 2017). The much larger Antarctic IESL component in ANU-ICE results in larger RSL sensitivities when shifts of the

IESLs were applied (Fig. S6E & F). We are not able to constrain the Antarctica IESL in this study, but more highstand data from the regions we identified (e.g., northern east coast and central west coast of Malay-Thai Peninsula, east coast of Sumatra) can provide better constraints and narrow down the uncertainty of IESL contribution from Antarctic (e.g., Jones et al., 2022).

7 Conclusions

We investigate the mid-Holocene sea-level highstand sensitivities to Earth and ice model parameters in GIA modelling in Singapore and Southeast Asia and compare model predictions with standardized RSL data from Singapore. We test a wide range of Earth model parameters and produce a mid-Holocene highstand "treasure map" considering the topography change and accommodation space to identify regions that may have highstand record preservation, which are validated with a peak highstand database compiled for Southeast Asia. Fixed with the ICE-6G_C ice model, our results show:

1. Earth model variation only affects the magnitude of the mid-Holocene highstand unless extraordinarily low upper mantle viscosity is used (e.g., $<4.0 \times 10^{19}$ Pa s), which leads to a shift of the timing of the highstand towards present and an absence of the highstand when upper mantle viscosity $\leq 1.0 \times 10^{19}$ Pa s.
2. The magnitude of the mid-Holocene highstand is sensitive to upper mantle viscosity and lower mantle viscosity especially when the lower mantle is $<1.0 \times 10^{22}$ Pa. In contrast, the mid-Holocene highstand magnitude is relatively insensitive to the lithospheric thickness.
3. Ice model variation can change both the timing and magnitude of the mid-Holocene highstand. Using the same Earth model, delaying the IESL will shift the timing of the highstand later and result in a lower highstand magnitude.
4. The highstand along the coasts of inner Sundaland, including west and east coasts of Malay-Thai Peninsula, east coast of Sumatra, and west coast of Borneo, are sensitive to upper (1D) and lower (both 1D and 3D) mantle viscosities.
5. The highstand "treasure map" shows that northern east coast and central west coast of Malay-Thai Peninsula, east coast of Sumatra, north coast of Java, and southwest coast of Borneo are very likely (90% probability) to have the mid-Holocene highstand preservation.

Our conclusions listed above are also supported by the ANU-ICE model applying the same group of Earth models, although the ANU-ICE model consistently predicts later timing by ~0.5 ka and lower magnitude by ~1 m of the mid-Holocene highstand, which are largely due to different Antarctic IESLs embedded within the ICE-6G_C and ANU-ICE models (Argus et al., 2014; Lambeck et al., 2014, 2017; Peltier et al., 2015).

Acknowledgments

We thank W. Richard Peltier for providing the ICE-6G_C ice model and Kurt Lambeck and Anthony Purcell for providing the ANU-ICE ice model. The global ANU-ICE combination model used in this study was kindly provided by Holger Steffen. Tanghua Li, Stephen Chua and Benjamin P. Horton are supported by the Singapore Ministry of Education Academic Research Fund MOE2019-T3-1-004 and MOE-T2EP50120-0007, the National Research Foundation Singapore, and the Singapore Ministry of Education, under the Research Centers of Excellence initiative. This research is also supported by the National Research Foundation, Singapore, and National Environment Agency, Singapore under the National Sea Level Programme Funding Initiative (award No. USS-IF-2020-1). Any opinions, findings and conclusions or recommendations expressed in this material are those of the author(s) and do not reflect the views of the National Research Foundation, Singapore and the National Environment Agency, Singapore. This research is conducted in part using the research computing facilities and/or advisory services offered by Information Technology Services, the University of Hong Kong. We express our gratitude to Muhammad Hadi Ikhsan for support with the graphics. This work is Earth Observatory of Singapore contribution number 538.

Figures

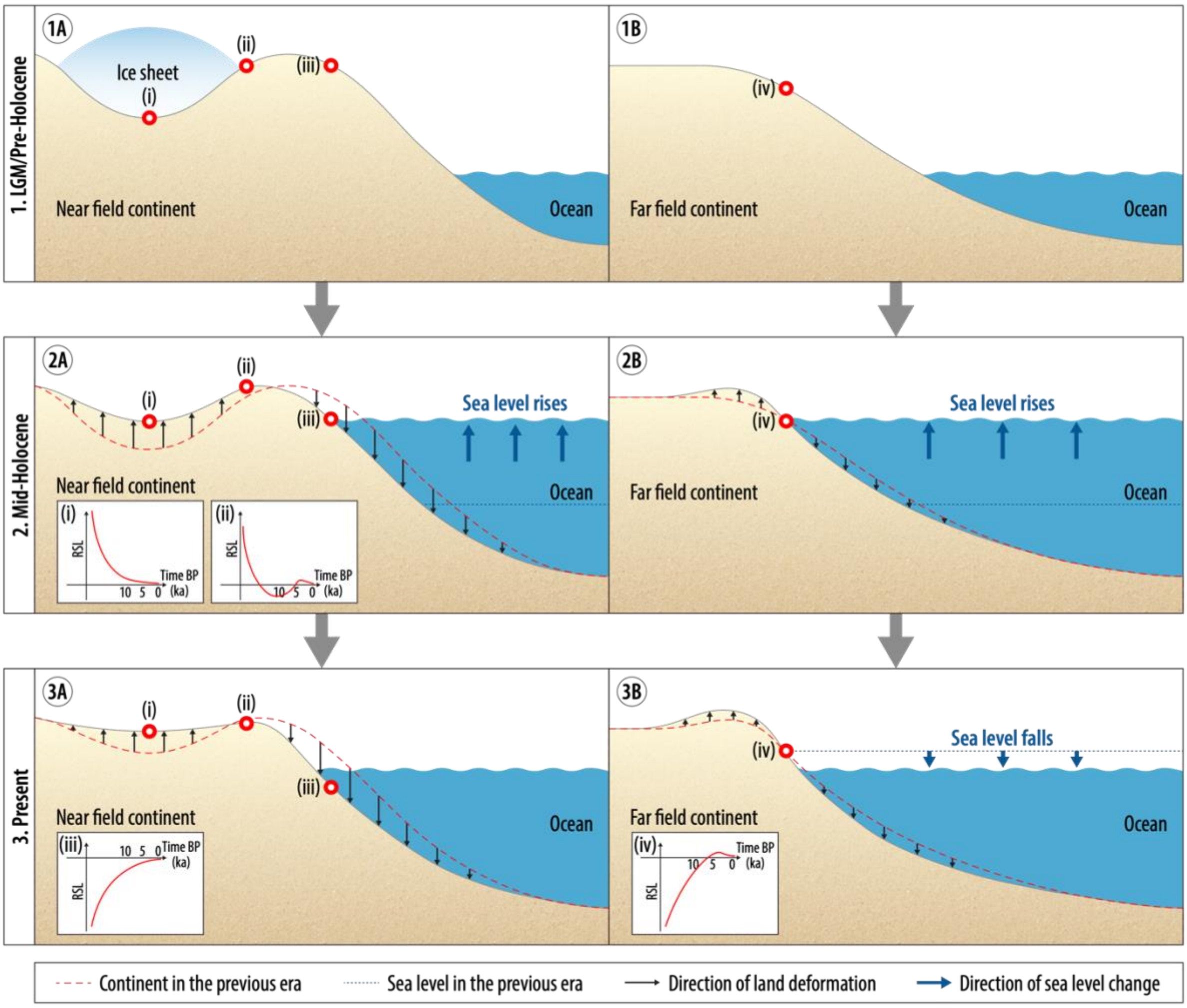

Fig. 1. Schematic of Glacial Isostatic Adjustment process at three stages (Last Glacial Maximum (LGM)/pre-Holocene, mid-Holocene and present), illustrating the equatorial ocean syphoning (panel A) and continental levering (panel B) mechanisms that induce the mid-Holocene sea-level highstand. Insets i-iv demonstrate the sea-level change pattern since LGM till present at locations in (i) near-field close to former ice sheet center (e.g., Hudson Bay, Canada), (ii) near-field close the former ice sheet margin (e.g., Andoy, Norway), (iii) intermediate-field near the forebulge (e.g., New Jersey, U.S.), (iv) far-field (e.g., Singapore).

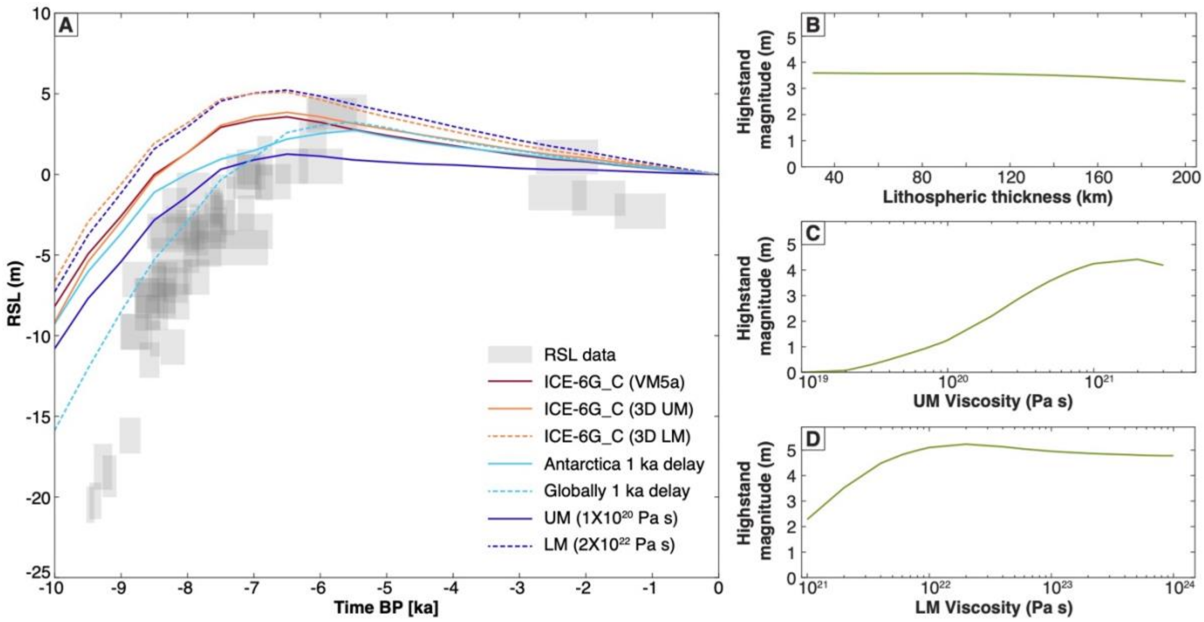

Fig. 2. (A) Reconstructed relative sea-level (RSL) data from Singapore (Chua et al., 2021) compared with RSL predictions of Glacial Isostatic Adjustment (GIA) model ICE-6G_C (VM5a) and other models that are modified from ICE-6G_C (VM5a). The predicted magnitude of the mid-Holocene highstand in GIA models with different (B) lithospheric thicknesses, (C) upper mantle (UM) viscosities, and (D) lower mantle (LM) viscosities fixed with the ICE-6G_C ice model.

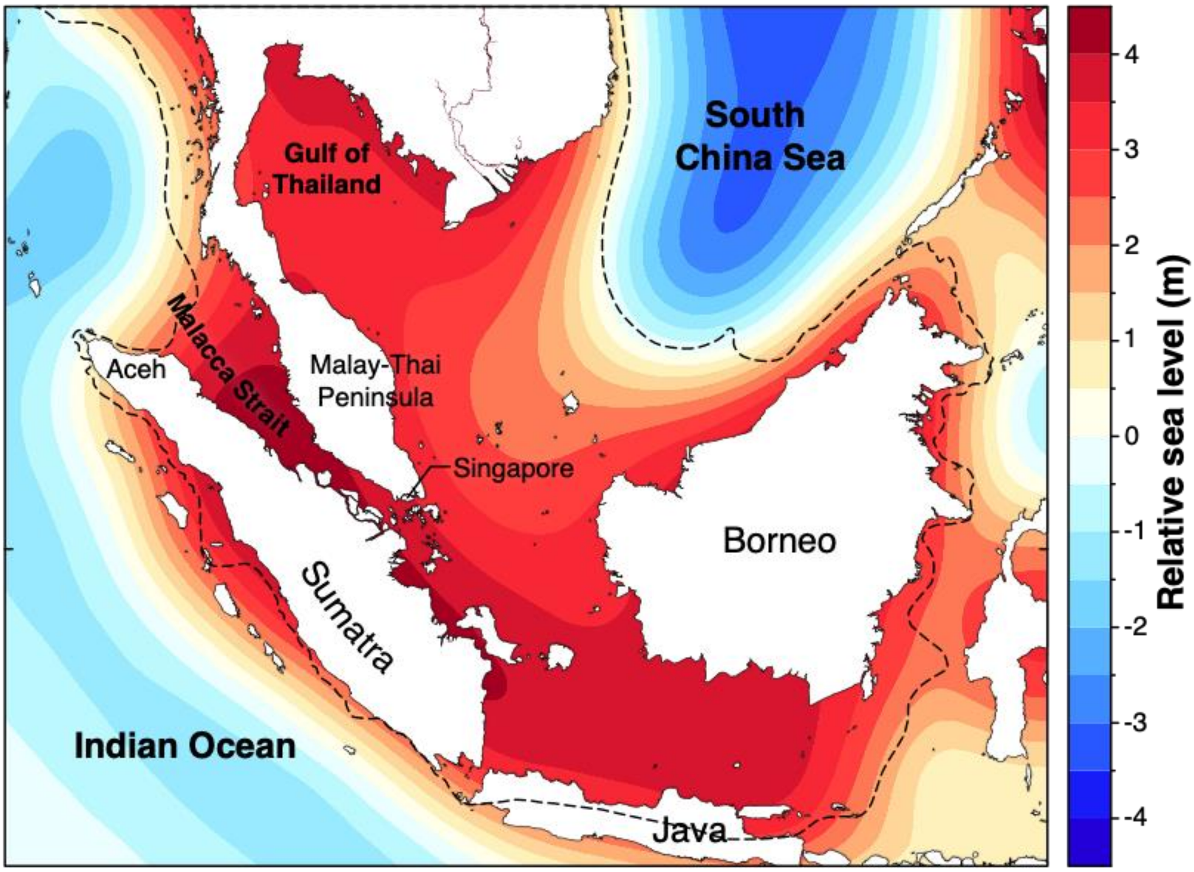

Fig. 3. Relative sea-level predictions of Glacial Isostatic Adjustment model ICE-6G_C (VM5a) in Southeast Asia at 6.5 ka BP. Positive RSL means above present-day sea level. The dotted line indicates the boundary for Sundaland (Hall, 2013).

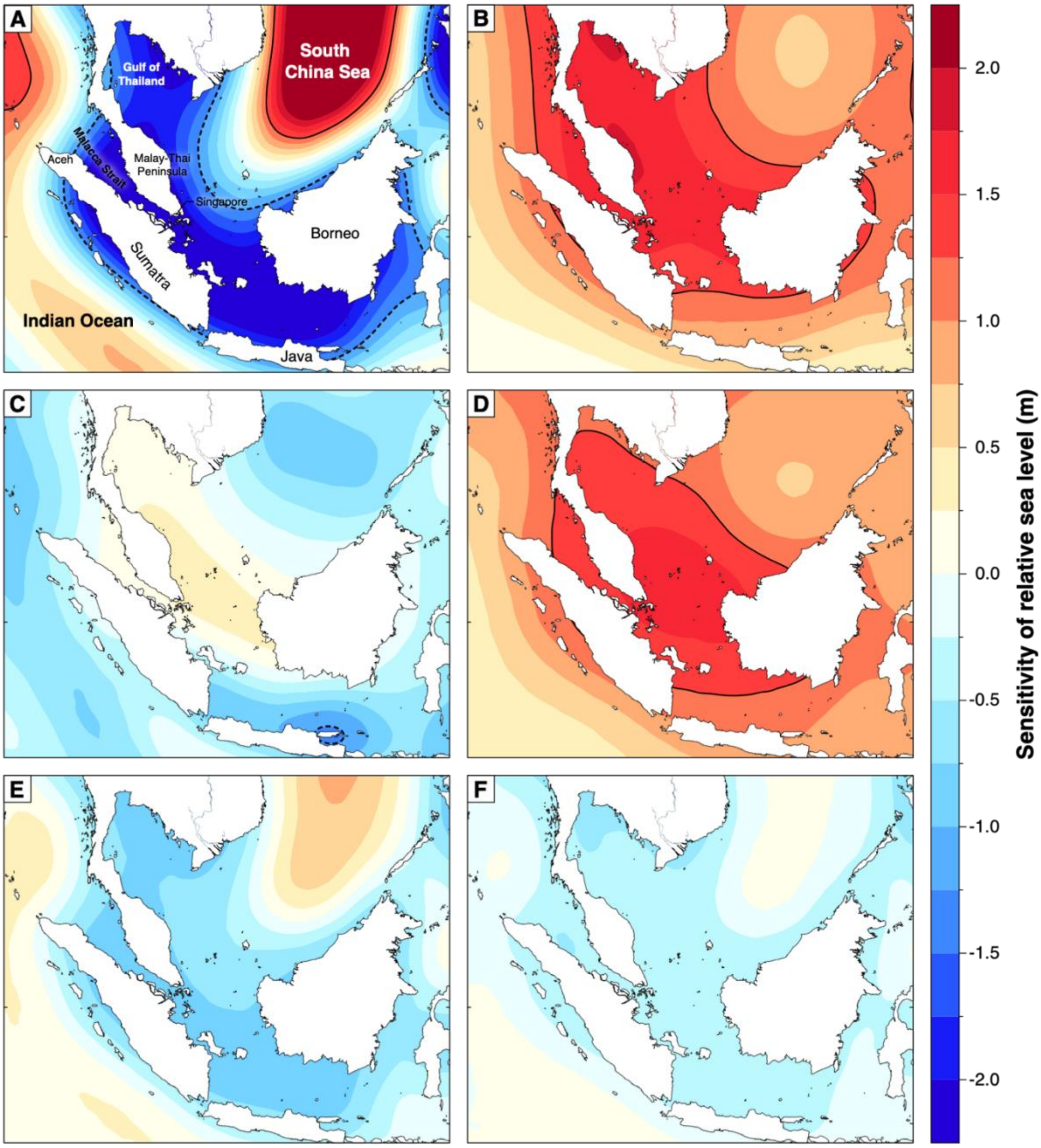

Fig. 4. Relative sea-level (RSL) sensitivity to (A) 1D upper mantle viscosity (1.0×10^{20} Pa s), (B) 1D lower mantle viscosity (2.0×10^{22} Pa s), (C) 3D upper mantle viscosity, (D) 3D lower mantle viscosity at 6.5 ka BP in Southeast Asia. RSL peak highstand sensitivity to 1 ka delay of (E) Antarctic and (F) global ice-equivalent sea-level (IESL) in Southeast Asia ($RSL_{Test}(5.5) - RSL_{Ref}(6.5)$). The black dashed and solid lines indicate the -1.25 m and 1.25 m contour lines, respectively.

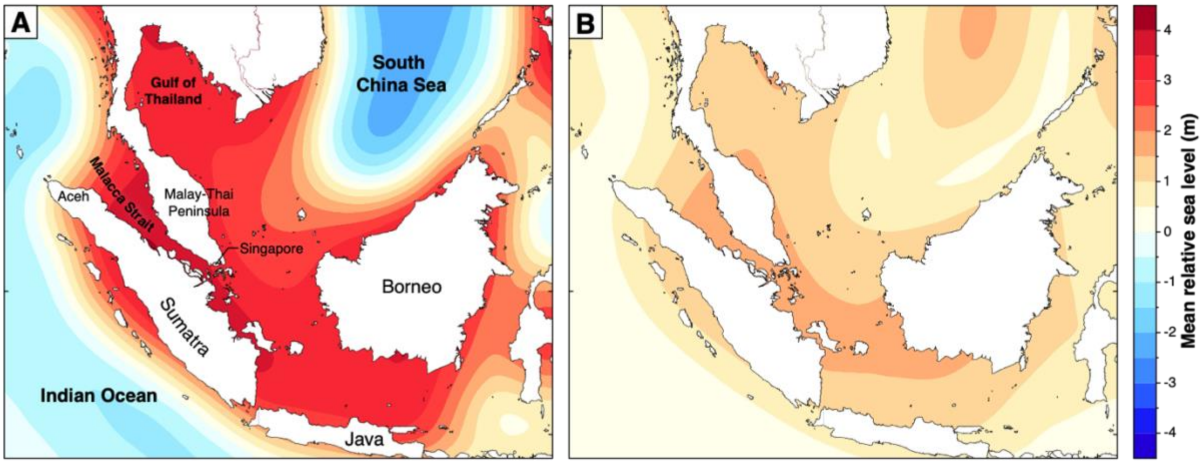

Fig. 5. (A) Mean relative sea level and (B) its standard deviation at 6.5 ka BP in Southeast Asia calculated from the Glacial Isostatic Adjustment model ensemble consisting of 45 1D models and 2 3D models with ICE-6G_C ice model. Note that A and B share the same scale on the right.

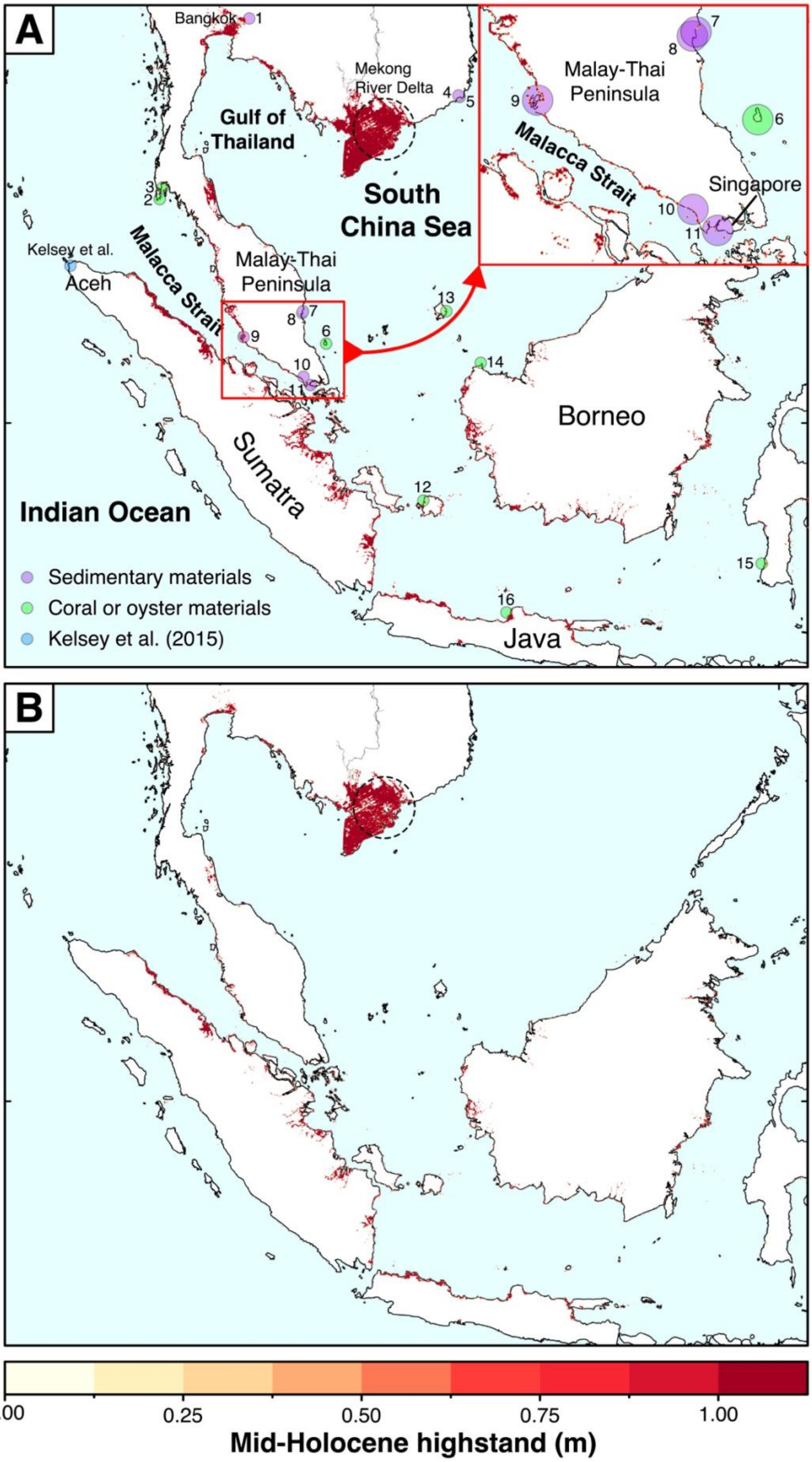
A
Bangkok
1
Mekong
River Delta
4
5
Gulf of
Thailand
South
China Sea
3
2
Kelsey et al.
Aceh
Malacca Strait
Malay-Thai
Peninsula
8
7
9
6
10
11
13
14
12
Borneo
Sumatra
Indian Ocean
Sedimentary materials
Coral or oyster materials
Kelsey et al. (2015)
15
16
Java
Malay-Thai
Peninsula
Malacca Strait
Singapore
B
0.00
0.25
0.50
0.75
1.00
Mid-Holocene highstand (m)

517

Fig. 6. Regions that are (A) likely (67% probability) and (B) very likely (90% probability) to have highstand record preservation considering topography change and accommodation space across Southeast Asia. The peak highstand data summarized in Table 1 are shown in purple and green dots for sedimentary and coral or oyster materials, respectively. The sea-level reconstruction site in Aceh from Kelsey et al. (2015) showing no evidence of a highstand is shown in blue dot.

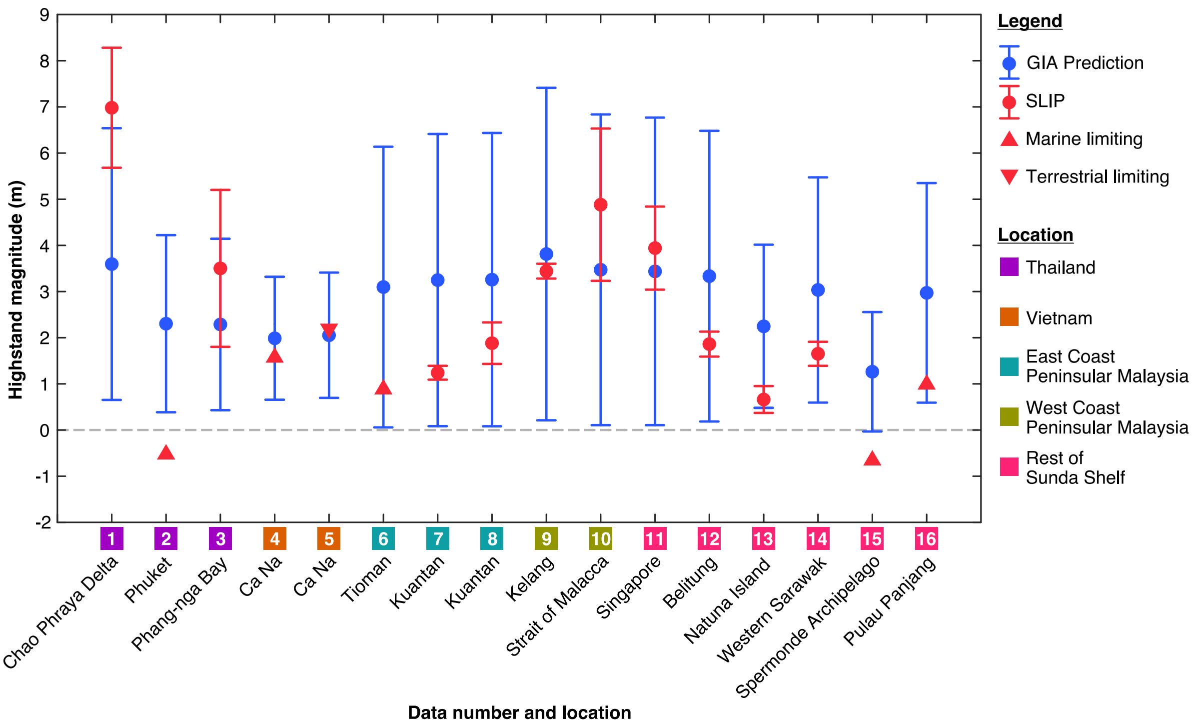

Fig. 7. The mid-Holocene peak highstand data with 2σ relative sea-level (RSL) uncertainties summarized in Table 1 are compared with the peak Glacial Isostatic Adjustment (GIA) highstand predictions with 2σ uncertainties (as shown in Figure 5). Note that the limiting data are plotted conservatively. The upwards (downwards) triangle represents the 2σ lower (upper) limit of the RSL uncertainty, indicating that RSL could be anywhere at or above (below) the flat part of the upwards (downwards) triangle. Note that the timing of peak highstand data points might be different from that of the peak GIA highstand predictions (e.g., 6.5 ka BP with ICE-6G_C), the magnitude of the highstand should be no lower than (i.e., equal or higher than) the peak highstand data showing here.

536 ## Tables

537 **Table 1 Southeast Asia mid-Holocene (7 – 4 ka BP) sea-level highstand database**

Location	Data No	Lat	Lon	Age (cal yr BP, 2 sigma)*	Material Indicator Type	Highstand RSL (m MSL)	Highstand Uncertainty + (m)	Highstand Uncertainty - (m)	Type	Reference
Thailand										
Chao Phraya Delta	1	13.92	101.58	7578 - 6194	Basal peat (mangrove)	6.98	1.30	1.30	SLIP	Somboon & Thiramongkol (1992)
Phuket	2	7.75	98.42	6611 - 6122	Coral	0.17	0.81	0.81	Marine limiting	Scoffin & Le Tissier (1998)
Phang-nga Bay	3	8.19	98.49	5924 - 5486	Rock oyster	3.50	1.70	1.70	SLIP	Scheffers et al. (2012)
Vietnam										
Southeast Vietnam (Ca Na)	4	11.33	108.83	6776 - 6423	Beach rock	2.11	0.57	0.57	Marine limiting	Stattegger et al. (2013)
Southeast Vietnam (Ca Na)	5	11.32	108.87	7275 - 6929	Beach ridge	1.58	0.67	0.67	Terrestrial limiting	Stattegger et al. (2013)
East Coast Peninsular Malaysia										
Tioman	6	2.72	104.17	6004 - 5315	Calcareous algae	1.74	0.97	0.97	Marine limiting	Tjia et al. (1983)
Kuantan	7	3.72	103.27	4817 - 4098	Back mangrove	1.24	0.15	0.15	SLIP	Hassan (2001)
Kuantan	8	3.70	103.25	4414 - 4160	Mangrove sediment	1.84	0.45	0.45	SLIP	Zhang et al. (2021)
West Coast Peninsular Malaysia										
Kelang (Strait of Malacca)	9	2.99	101.50	6390 - 5898	Mangrove peat	3.44	0.16	0.15	SLIP	Hassan (2001)
Strait of Malacca	10	1.62	103.42	4862 - 4097	Mangrove peat	4.88	1.65	1.65	SLIP	Geyh et al. (1979)
Rest of Sunda shelf										
Singapore	11	1.36	103.69	6270 - 5330	Upper intertidal deposit	3.94	0.90	0.88	SLIP	Bird et al. (2010)
Belitung	12	-2.70	107.62	6849 - 6480	Coral microatoll	1.86	0.27	0.27	SLIP	Meltzner et al. (2017)
Natuna Island	13	3.90	108.40	4702 – 4680	Coral microatoll	0.66	0.29	0.29	SLIP	Wan et al. (2020)
Western Sarawak coast of Borneo	14	2.06	109.65	6087 – 6037	Coral microatoll	1.65	0.25	0.25	SLIP	Majewski et al. (2018)
Spermonde Archipelago, Makassar Strait	15	-4.95	119.36	6122 - 5756	Coral microatoll (eroded)	-0.66	0.11	0.11	Marine limiting	Mann et al. (2016)
Pulau Panjang, Java	16	-6.58	110.62	6547 - 6337	Coral microatoll (eroded)	1.06	0.18	0.18	Marine limiting	Mann et al. (2023)

539 *: All 14C ages recalibrated using IntCal20 and Marine20

References

Al-Mikhlafi, A. S., Hibbert, F. D., Edwards, L. R., & Cheng, H. (2021). Holocene relative sea-level changes and coastal evolution along the coastlines of Kamaran Island and As-Salif Peninsula, Yemen, southern Red Sea. *Quaternary Science Reviews*, *252*, 106719.

Angulo, R. J., Lessa, G. C., & de Souza, M. C. (2006). A critical review of mid-to late-Holocene sea-level fluctuations on the eastern Brazilian coastline. *Quaternary Science Reviews*, *25*(5–6), 486–506.

Anthony, E. J., Brunier, G., Besset, M., Goichot, M., Dussouillez, P., & Nguyen, V. L. (2015). Linking rapid erosion of the Mekong River delta to human activities. *Scientific Reports*, *5*(1), 1–12.

Argus, D. F., Peltier, W. R., Drummond, R., & Moore, A. W. (2014). The Antarctica component of postglacial rebound model ICE-6G_C (VM5a) based on GPS positioning, exposure age dating of ice thicknesses, and relative sea level histories. *Geophysical Journal International*, *198*(1), 537–563. https://doi.org/10.1093/gji/ggu140

Bird, M. I., Austin, W. E. N., Wurster, C. M., Fifield, L. K., Mojtahid, M., & Sargeant, C. (2010). Punctuated eustatic sea-level rise in the early mid-Holocene. *Geology*, *38*(9), 803–806.

Bird, M. I., Fifield, L. K., Teh, T. S., Chang, C. H., Shirlaw, N., & Lambeck, K. (2007). An inflection in the rate of early mid-Holocene eustatic sea-level rise: A new sea-level curve from Singapore. *Estuarine, Coastal and Shelf Science*, *71*(3–4), 523–536.

Bradley, S. L., Milne, G. A., Horton, B. P., & Zong, Y. (2016). Modelling sea level data from China and Malay-Thailand to estimate Holocene ice-volume equivalent sea level change. *Quaternary Science Reviews*, *137*, 54–68.

Cheng, H., Edwards, R. L., Shen, C.-C., Polyak, V. J., Asmerom, Y., Woodhead, J., Hellstrom, J., Wang, Y., Kong, X., & Spötl, C. (2013). Improvements in 230Th dating, 230Th and 234U half-life values, and U–Th isotopic measurements by multi-collector inductively coupled plasma mass spectrometry. *Earth and Planetary Science Letters*, *371*, 82–91.

Chua, S., Switzer, A. D., Li, T., Chen, H., Christie, M., Shaw, T. A., Khan, N. S., Bird, M. I., & Horton, B. P. (2021). A new Holocene sea-level record for Singapore. *The Holocene*, *31*(9), 1376–1390.

Clark, J. A., Farrell, W. E., & Peltier, W. R. (1978). Global Changes in Postglacial Sea Level: A Numerical Calculation 1. *Quaternary Research*, *9*(3), 265–287.

Dura, T., Engelhart, S. E., Vacchi, M., Horton, B. P., Kopp, R. E., Peltier, W. R., & Bradley, S. (2016). The role of Holocene relative sea-level change in preserving records of subduction zone earthquakes. *Current Climate Change Reports*, *2*, 86–100.

Dutton, A., Carlson, A. E., Long, Aj., Milne, G. A., Clark, P. U., DeConto, R., Horton, B. P., Rahmstorf, S., & Raymo, M. E. (2015). Sea-level rise due to polar ice-sheet mass loss during past warm periods. *Science*, *349*(6244), aaa4019.

Fontes, N. A., Moraes, C. A., Cohen, M. C. L., Alves, I. C. C., França, M. C., Pessenda, L. C.

R., Francisquini, M. I., Bendassolli, J. A., Macario, K., & Mayle, F. (2017). The impacts of the middle Holocene high sea-level stand and climatic changes on mangroves of the Jucuruçu River, southern Bahia–northeastern Brazil. *Radiocarbon*, *59*(1), 215–230.

Geyh, M. A., Streif, H., & Kudrass, H.-R. (1979). Sea-level changes during the late Pleistocene and Holocene in the Strait of Malacca. *Nature*, *278*(5703), 441–443.

Grand, S. P. (2002). Mantle shear–wave tomography and the fate of subducted slabs. *Philosophical Transactions of the Royal Society of London. Series A: Mathematical, Physical and Engineering Sciences*, *360*(1800), 2475–2491. https://doi.org/10.1098/rsta.2002.1077

Hall, R., & Morley, C. K. (2004). Sundaland basins. *Continent-Ocean Interactions within East Asian Marginal Seas*, 55–85.

Hassan, K. (2002). Holocene sea level changes in Peninsular Malaysia. *Bulletin of the Geological Society of Malaysia*, *45*, 301–307.

Heaton, T. J., Köhler, P., Butzin, M., Bard, E., Reimer, R. W., Austin, W. E. N., Ramsey, C. B., Grootes, P. M., Hughen, K. A., & Kromer, B. (2020). Marine20—the marine radiocarbon age calibration curve (0–55,000 cal BP). *Radiocarbon*, *62*(4), 779–820.

Horton, B. P., Edwards, R. J., & Lloyd, J. M. (2000). Implications of a microfossil-based transfer function in Holocene sea-level studies. *Geological Society, London, Special Publications*, *166*(1), 41–54.

Horton, B. P., Gibbard, P. L., Milne, G. M., Morley, R. J., Purintavaragul, C., & Stargardt, J. M. (2005). *Holocene sea levels and Peninsula , southeast Asia*. *8*, 1199–1214.

Ioc, I. H. O. (2003). BODC: Centenary Edition of the GEBCO Digital Atlas, published on CD-ROM on behalf of the Intergovernmental Oceanographic Commission and the International Hydrographic Organization as part of the General Bathymetric Chart of the Oceans. *British Oceanographic Data Centre, Liverpool, UK*, *52*.

Jones, R. S., Johnson, J. S., Lin, Y., Mackintosh, A. N., Sefton, J. P., Smith, J. A., Thomas, E. R., & Whitehouse, P. L. (2022). Stability of the Antarctic Ice Sheet during the pre-industrial Holocene. *Nature Reviews Earth & Environment*, *3*(8), 500–515.

Joyse, K. M., Khan, N. S., Moyer, R. P., Radabaugh, K. R., Hong, I., Chappel, A. R., Walker, J. S., Sanders, C. J., Engelhart, S. E., & Kopp, R. E. (2023). The characteristics and preservation potential of Hurricane Irma's overwash deposit in southern Florida, USA. *Marine Geology*, 107077.

Kahlert, T., O'Donnell, S., Stimpson, C., Hương, N. T. M., Hill, E., Utting, B., & Rabett, R. (2021). Mid-Holocene coastline reconstruction from geomorphological sea level indicators in the Tràng An World Heritage Site, Northern Vietnam. *Quaternary Science Reviews*, *263*, 107001.

Kamaludin, H. (2001). Holocene sea level changes in Kelang and Kuantan, Peninsular Malaysia. *Ph. D. Thesis*, 309.

Kaufmann, G., Wu, P., & Wolf, D. (1997). Some effects of lateral heterogeneities in the upper mantle on postglacial land uplift close to continental margins. *Geophysical Journal International*, *128*(1), 175–187.

Kelsey, H. M., Engelhart, S. E., Pilarczyk, J. E., Horton, B. P., Rubin, C. M., Daryono, M. R., Ismail, N., Hawkes, A. D., Bernhardt, C. E., & Cahill, N. (2015). Accommodation space, relative sea level, and the archiving of paleo-earthquakes along subduction zones. *Geology*, *43*(8), 675–678.

Kendall, R., Mitrovica, J. X., & Sabadini, R. (2003). Lithospheric thickness inferred from Australian post-glacial sea-level change: The influence of a ductile crustal zone. *Geophysical Research Letters*, *30*(9).

Khan, N. S., Horton, B. P., Engelhart, S., Rovere, A., Vacchi, M., Ashe, E. L., Törnqvist, T. E., Dutton, A., Hijma, M. P., & Shennan, I. (2019). Inception of a global atlas of sea levels since the Last Glacial Maximum. *Quaternary Science Reviews*, *220*, 359–371. https://doi.org/10.1016/j.quascirev.2019.07.016

Kidson, C. (1982). Sea level changes in the Holocene. *Quaternary Science Reviews*, *1*(2), 121–151.

King, D. J., Newnham, R. M., Gehrels, W. R., & Clark, K. J. (2021). Late Holocene sea-level changes and vertical land movements in New Zealand. *New Zealand Journal of Geology and Geophysics*, *64*(1), 21–36.

Lambeck, K. (2002). Sea level change from mid Holocene to recent time: an Australian example with global implications. *Ice Sheets, Sea Level and the Dynamic Earth*, *29*, 33–50.

Lambeck, K., & Nakada, M. (1990). Late Pleistocene and Holocene sea-level change along the Australian coast. *Palaeogeography, Palaeoclimatology, Palaeoecology*, *89*(1–2), 143–176.

Lambeck, K., Purcell, A., Johnston, P., Nakada, M., & Yokoyama, Y. (2003). Water-load definition in the glacio-hydro-isostatic sea-level equation. *Quaternary Science Reviews*, *22*(2–4), 309–318.

Lambeck, K., Purcell, A., Zhao, J., & SVENSSON, N.-O. (2010). The Scandinavian ice sheet: from MIS 4 to the end of the Last Glacial Maximum. *Boreas*, *39*(2), 410–435.

Lambeck, K., Purcell, A., & Zhao, S. (2017). The North American Late Wisconsin ice sheet and mantle viscosity from glacial rebound analyses. *Quaternary Science Reviews*, *158*, 172–210. https://doi.org/10.1016/j.quascirev.2016.11.033

Lambeck, K., Rouby, H., Purcell, A., Sun, Y., & Sambridge, M. (2014). Sea level and global ice volumes from the Last Glacial Maximum to the Holocene. *Proceedings of the National Academy of Sciences*, *111*(43), 15296–15303. https://doi.org/10.1073/pnas.1411762111

Li, T., Khan, N. S., Baranskaya, A. V, Shaw, T. A., Peltier, W. R., Stuhne, G. R., Wu, P., & Horton, B. P. (2022). Influence of 3D Earth Structure on Glacial Isostatic Adjustment in the Russian Arctic. *Journal of Geophysical Research: Solid Earth*, *127*(3), e2021JB023631.

Li, T., & Wu, P. (2019). Laterally heterogeneous lithosphere, asthenosphere and sub-lithospheric properties under Laurentia and Fennoscandia from Glacial Isostatic Adjustment. *Geophysical Journal International*, *216*(3), 1633–1647. https://doi.org/10.1093/gji/ggy475

Li, T., Wu, P., Steffen, H., & Wang, H. (2018). In search of laterally heterogeneous viscosity models of glacial isostatic adjustment with the ICE-6G_C global ice history model. *Geophysical Journal International*, *214*(2), 1191–1205. https://doi.org/10.1093/gji/ggy181

Li, T., Wu, P., Wang, H., Steffen, H., Khan, N. S., Engelhart, S. E., Vacchi, M., Shaw, T. A., Peltier, W. R., & Horton, B. P. (2020). Uncertainties of Glacial Isostatic Adjustment model predictions in North America associated with 3D structure. *Geophysical Research Letters*, e2020GL087944. https://doi.org/10.1029/2020GL087944

Li, Z., Saito, Y., Mao, L., Tamura, T., Song, B., Zhang, Y., Lu, A., Sieng, S., & Li, J. (2012). Mid-Holocene mangrove succession and its response to sea-level change in the upper Mekong River delta, Cambodia. *Quaternary Research*, *78*(2), 386–399.

Liberatore, M., Gliozzi, E., Cipollari, P., Öğretmen, N., Spada, G., & Cosentino, D. (2022). Vertical velocity fields along the Eastern Mediterranean coast as revealed by late Holocene sea-level markers. *Earth-Science Reviews*, 104199.

Lin, Y., Hibbert, F. D., Whitehouse, P. L., Woodroffe, S. A., Purcell, A., Shennan, I., & Bradley, S. L. (2021). A reconciled solution of Meltwater Pulse 1A sources using sea-level fingerprinting. *Nature Communications*, *12*(1), 1–11.

Liu, J., Milne, G. A., Kopp, R. E., Clark, P. U., & Shennan, I. (2016). Sea-level constraints on the amplitude and source distribution of Meltwater Pulse 1A. *Nature Geoscience*, *9*(2), 130–134.

Lokier, S. W., Bateman, M. D., Larkin, N. R., Rye, P., & Stewart, J. R. (2015). Late Quaternary sea-level changes of the Persian Gulf. *Quaternary Research*, *84*(1), 69–81.

Majewski, J. M., Switzer, A. D., Meltzner, A. J., Parham, P. R., Horton, B. P., Bradley, S. L., Pile, J., Chiang, H.-W., Wang, X., & Ng, C. T. (2018). Holocene relative sea-level records from coral microatolls in Western Borneo, South China Sea. *The Holocene*, *28*(9), 1431–1442.

Mann, T., Bender, M., Lorscheid, T., Stocchi, P., Vacchi, M., Switzer, A. D., & Rovere, A. (2019). Holocene sea levels in southeast Asia, Maldives, India and Sri Lanka: the SEAMIS database. *Quaternary Science Reviews*, *219*, 112–125.

Mann, T., Rovere, A., Schöne, T., Klicpera, A., Stocchi, P., Lukman, M., & Westphal, H. (2016). The magnitude of a mid-Holocene sea-level highstand in the Strait of Makassar. *Geomorphology*, *257*, 155–163.

Mann, T., Schöne, T., Kench, P., Lambeck, K., Ashe, E., Kneer, D., Beetham, E., Illigner, J., Rovere, A., & Marfai, M. A. (2023). Fossil Java Sea corals record Laurentide ice sheet disappearance. *Geology*.

Mauz, B., Ruggieri, G., & Spada, G. (2015). Terminal Antarctic melting inferred from a far-field coastal site. *Quaternary Science Reviews*, *116*, 122–132.

Mauz, B., Shen, Z., Alsuwaidi, M., Melini, D., Spada, G., & Purkis, S. J. (2022). The mid-Holocene sea-level change in the Arabian Gulf. *The Holocene*, *32*(11), 1173–1183.

Melini, D., & Spada, G. (2019). Some remarks on Glacial Isostatic Adjustment modelling uncertainties. *Geophysical Journal International*, *218*(1), 401–413.

Meltzner, A. J., Switzer, A. D., Horton, B. P., Ashe, E., Qiu, Q., Hill, D. F., Majewski, M., & Natawidjaja, D. H. (2017). *Half-metre sea-level fluctuations on centennial timescales from mid-Holocene corals of Southeast Asia*. https://doi.org/10.1038/ncomms14387

Milne, G. A., Long, A. J., & Bassett, S. E. (2005). Modelling Holocene relative sea-level observations from the Caribbean and South America. *Quaternary Science Reviews*, *24*(10–11), 1183–1202.

Mitrovica, J X, & Forte, A. M. (2004). A new inference of mantle viscosity based upon joint inversion of convection and glacial isostatic adjustment data. *Earth and Planetary Science Letters*, *225*(1–2), 177–189.

Mitrovica, J X, & Milne, G. A. (2002). On the origin of late Holocene sea-level highstands within equatorial ocean basins. *Quaternary Science Reviews*, *21*(20–22), 2179–2190.

Mitrovica, Jerry X, & Peltier, W. R. (1991). On postglacial geoid subsidence over the equatorial oceans. *Journal of Geophysical Research: Solid Earth*, *96*(B12), 20053–20071.

Nakada, M., & Lambeck, K. (1989). Late Pleistocene and Holocene sea-level change in the Australian region and mantle rheology. *Geophysical Journal International*, *96*(3), 497–517.

Natawidjaja, D. H., Sieh, K., Galetzka, J., Suwargadi, B. W., Cheng, H., Edwards, R. L., & Chlieh, M. (2007). Interseismic deformation above the Sunda Megathrust recorded in coral microatolls of the Mentawai islands, West Sumatra. *Journal of Geophysical Research: Solid Earth*, *112*(B2).

Nguyen, V. L., Ta, T. K. O., & Saito, Y. (2010). Early Holocene initiation of the Mekong River delta, Vietnam, and the response to Holocene sea-level changes detected from DT1 core analyses. *Sedimentary Geology*, *230*(3–4), 146–155.

Nunn, P. D., & Peltier, W. R. (2001). Far-field test of the ICE-4G model of global isostatic response to deglaciation using empirical and theoretical Holocene sea-level reconstructions for the Fiji Islands, southwestern Pacific. *Quaternary Research*, *55*(2), 203–214.

Peltier, W R. (2004). Global glacial isostasy and the surface of the ice-age Earth: the ICE-5G (VM2) model and GRACE. *Annu. Rev. Earth Planet. Sci.*, *32*, 111–149.

Peltier, W R, Argus, D. F., & Drummond, R. (2015). Space geodesy constrains ice age terminal deglaciation: The global ICE-6G_C (VM5a) model. *Journal of Geophysical Research: Solid Earth*, *120*(1), 450–487. https://doi.org/10.1002/2014JB011176

Peltier, W R, Wu, P. P.-C., Argus, D., Li, T., & Velay-Vitow, J. (2022). Glacial Isostatic Adjustment: Physical Models and Observational Constraints. *Reports on Progress in Physics*.

Peltier, W Richard. (1994). Ice age paleotopography. *Science*, *265*(5169), 195–201.

Pirazzoli, P. A. (2005). A review of possible eustatic, isostatic and tectonic contributions in eight late-Holocene relative sea-level histories from the Mediterranean area. *Quaternary Science Reviews*, *24*(18–19), 1989–2001.

Powell, E. M., Pan, L., Hoggard, M. J., Latychev, K., Gomez, N., Austermann, J., & Mitrovica,

J. X. (2021). The impact of 3-D Earth structure on far-field sea level following interglacial West Antarctic Ice Sheet collapse. *Quaternary Science Reviews*, *273*, 107256.

Ramsey, C. B. (2001). Development of the radiocarbon calibration program. *Radiocarbon*, *43*(2A), 355–363.

Reimer, P. J., Austin, W. E. N., Bard, E., Bayliss, A., Blackwell, P. G., Ramsey, C. B., Butzin, M., Cheng, H., Edwards, R. L., & Friedrich, M. (2020). The IntCal20 Northern Hemisphere radiocarbon age calibration curve (0–55 cal kBP). *Radiocarbon*, *62*(4), 725–757.

Reimer, P. J., & Reimer, R. W. (2001). A marine reservoir correction database and on-line interface. *Radiocarbon*, *43*(2A), 461–463.

Sasgen, I., Martín-Español, A., Horvath, A., Klemann, V., Petrie, E. J., Wouters, B., Horwath, M., Pail, R., Bamber, J. L., & Clarke, P. J. (2017). Joint inversion estimate of regional glacial isostatic adjustment in Antarctica considering a lateral varying Earth structure (ESA STSE Project REGINA). *Geophysical Journal International*, *211*(3), 1534–1553.

Scheffers, A., Brill, D., Kelletat, D., Brückner, H., Scheffers, S., & Fox, K. (2012). Holocene sea levels along the Andaman Sea coast of Thailand. *The Holocene*, *22*(10), 1169–1180.

Scoffin, T. P., & Le Tissier, M. D. A. (1998). Late Holocene sea level and reef-flat progradation, Phuket, South Thailand. *Coral Reefs*, *17*(3), 273–276.

Sefton, J. P., Kemp, A. C., Engelhart, S. E., Ellison, J. C., Karegar, M. A., Charley, B., & McCoy, M. D. (2022). Implications of anomalous relative sea-level rise for the peopling of Remote Oceania. *Proceedings of the National Academy of Sciences*, *119*(52), e2210863119.

Shennan, I, & Horton, B. P. (2002). Relative sea-level changes and crustal movements of the UK. *Journal of Quaternary Science*, *16*(5–6), 511–526.

Shennan, Ian. (1986). Flandrian sea-level changes in the Fenland. II: Tendencies of sea-level movement, altitudinal changes, and local and regional factors. *Journal of Quaternary Science*, *1*(2), 155–179.

Shennan, Ian, Long, A. J., & Horton, B. P. (2015). *Handbook of sea-level research*. John Wiley & Sons.

Sinsakul, S. (2000). Late quaternary geology of the lower central plain, Thailand. *Journal of Asian Earth Sciences*, *18*(4), 415–426.

Somboon, J. R. P., & Thiramongkol, N. (1992). Holocene highstand shoreline of the Chao Phraya delta, Thailand. *Journal of Southeast Asian Earth Sciences*, *7*(1), 53–60.

Stattegger, K., Tjallingii, R., Saito, Y., Michelli, M., Thanh, N. T., & Wetzel, A. (2013). Mid to late Holocene sea-level reconstruction of Southeast Vietnam using beachrock and beach-ridge deposits. *Global and Planetary Change*, *110*, 214–222.

Steffen, H., Wu, P., & Wang, H. (2014). Optimal locations of sea-level indicators in glacial isostatic adjustment investigations. *Solid Earth*, *5*(1), 511.

Subarya, C., Chlieh, M., Prawirodirdjo, L., Avouac, J.-P., Bock, Y., Sieh, K., Meltzner, A. J., Natawidjaja, D. H., & McCaffrey, R. (2006). Plate-boundary deformation associated with the great Sumatra–Andaman earthquake. *Nature*, *440*(7080), 46–51.

Tam, C., Zong, Y., Xiong, H., Wu, P., Sun, Y., & Huang, G. (2018). A below-the-present late Holocene relative sea level and the glacial isostatic adjustment during the Holocene in the Malay Peninsula. *Quaternary Science Reviews*, *201*, 206–222. https://doi.org/10.1016/j.quascirev.2018.10.009

Tamura, T., Saito, Y., Nguyen, V. L., Ta, T. K. O., Bateman, M. D., Matsumoto, D., & Yamashita, S. (2012). Origin and evolution of interdistributary delta plains; insights from Mekong River delta. *Geology*, *40*(4), 303–306.

Tan, F., Khan, N. S., Li, T., Meltzner, A. J., Majewski, J., Chan, N., Chutcharavan, P. M., Cahill, N., Vacchi, M., & Peng, D. (2023). Holocene relative sea-level histories of far-field islands in the mid-Pacific. *Quaternary Science Reviews*, 107995.

Tjallingii, R., Stattegger, K., Stocchi, P., Saito, Y., & Wetzel, A. (2014). Rapid flooding of the southern Vietnam shelf during the early to mid-Holocene. *Journal of Quaternary Science*, *29*(6), 581–588.

Tjallingii, R., Stattegger, K., Wetzel, A., & Van Phach, P. (2010). Infilling and flooding of the Mekong River incised valley during deglacial sea-level rise. *Quaternary Science Reviews*, *29*(11–12), 1432–1444.

Tjia, H D, Fujii, S., & Kigoshi, K. (1983). Holocene shorelines of Tioman island in the South China sea. *Geologie En Mijnbouw*, *62*(4), 599–604.

Tjia, Hong Djin. (1996). Sea-level changes in the tectonically stable Malay-Thai Peninsula. *Quaternary International*, *31*, 95–101.

Törnqvist, T. E., Cahoon, D. R., Morris, J. T., & Day, J. W. (2021). Coastal wetland resilience, accelerated sea-level rise, and the importance of timescale. *AGU Advances*, *2*(1), e2020AV000334.

Van de Plassche, O. (1986). Sea-level research: A manual for the collection and evaluation of data: Norwich. *UK, Geobooks*.

Walcott, R. I. (1972). Past sea levels, eustasy and deformation of the earth. *Quaternary Research*, *2*(1), 1–14.

Wan, J. X. W., Meltzner, A. J., Switzer, A. D., Lin, K., Wang, X., Bradley, S. L., Natawidjaja, D. H., Suwargadi, B. W., & Horton, B. P. (2020). Relative sea-level stability and the radiocarbon marine reservoir correction at Natuna Island, Indonesia, since 6400 yr BP. *Marine Geology*, *430*, 106342.

Wang, F., Zong, Y., Mauz, B., Li, J., Fang, J., Tian, L., Chen, Y., Shang, Z., Jiang, X., & Spada, G. (2020). Holocene sea-level change on the central coast of Bohai Bay, China. *Earth Surface Dynamics*, *8*(3), 679–693.

Wu, P. (2004). Using commercial finite element packages for the study of earth deformations, sea levels and the state of stress. *Geophysical Journal International*, *158*(2), 401–408.

Wu, P. (2006). Sensitivity of relative sea levels and crustal velocities in Laurentide to radial and lateral viscosity variations in the mantle. *Geophysical Journal International*, *165*(2), 401–413. https://doi.org/10.1111/j.1365-246X.2006.02960.x

Xiong, H., Zong, Y., Li, T., Long, T., & Huang, G. (2020). Coastal GIA processes revealed by the early to middle Holocene sea- level history of east China. *Quaternary Science Reviews*, *233*, 106249. https://doi.org/10.1016/j.quascirev.2020.106249

Yamano, H., Inoue, T., Adachi, H., Tsukaya, K., Adachi, R., & Baba, S. (2019). Holocene sea-level change and evolution of a mixed coral reef and mangrove system at Iriomote Island, southwest Japan. *Estuarine, Coastal and Shelf Science*, *220*, 166–175.

Yokoyama, Y., Okuno, J., Miyairi, Y., Obrochta, S., Demboya, N., Makino, Y., & Kawahata, H. (2012). Holocene sea-level change and Antarctic melting history derived from geological observations and geophysical modeling along the Shimokita Peninsula, northern Japan. *Geophysical Research Letters*, *39*(13).

Yokoyama, Y., & Purcell, A. (2021). On the geophysical processes impacting palaeo-sea-level observations. *Geoscience Letters, 8*(1), 1–19.

Yousefi, M., Milne, G. A., Love, R., & Tarasov, L. (2018). Glacial isostatic adjustment along the Pacific coast of central North America. *Quaternary Science Reviews*, *193*, 288–311.

Yu, F., Li, N., Tian, G., Huang, Z., Xiong, H., Li, T., Liu, S., & Liu, Y. (2023). A re-evaluation of Holocene relative sea-level change along the Fujian coast, southeastern China. *Palaeogeography, Palaeoclimatology, Palaeoecology*, 111577.

Zhang, Y., Zong, Y., Xiong, H., Li, T., Fu, S., Huang, G., & Zheng, Z. (2021). The middle-to-late Holocene relative sea-level history, highstand and levering effect on the east coast of Malay Peninsula. *Global and Planetary Change*, *196*, 103369.

Zoccarato, C., Minderhoud, P. S. J., & Teatini, P. (2018). The role of sedimentation and natural compaction in a prograding delta: insights from the mega Mekong delta, Vietnam. *Scientific Reports*, *8*(1), 1–12.

Supplementary Information for

Glacial Isostatic Adjustment modelling of the mid-Holocene sea-level highstand of Singapore and Southeast Asia

Tanghua Li[1*], Stephen Chua[1,a], Fangyi Tan[1,2,a], Nicole S. Khan[3], Timothy Shaw[1], Jędrzej Majewski[1], Aron Meltzner[1,3], Adam Switzer[1,3], Patrick Wu[4], and Benjamin P. Horton[1,3]

[1]Earth Observatory of Singapore, Nanyang Technological University, Singapore, Singapore

[2]Asian School of the Environment, Nanyang Technological University, Singapore, Singapore

[3]Department of Earth Sciences and the Swire Institute of Marine Science, University of Hong Kong, Hong Kong, China

[4]Department of Geoscience, University of Calgary, Calgary, Alberta, Canada

[a] The authors contributed equally

*Corresponding author: Tanghua Li (li.tanghua@ntu.edu.sg)

Contents of this file

Figures S1 to S8

Table S1 to S2

Text S1.

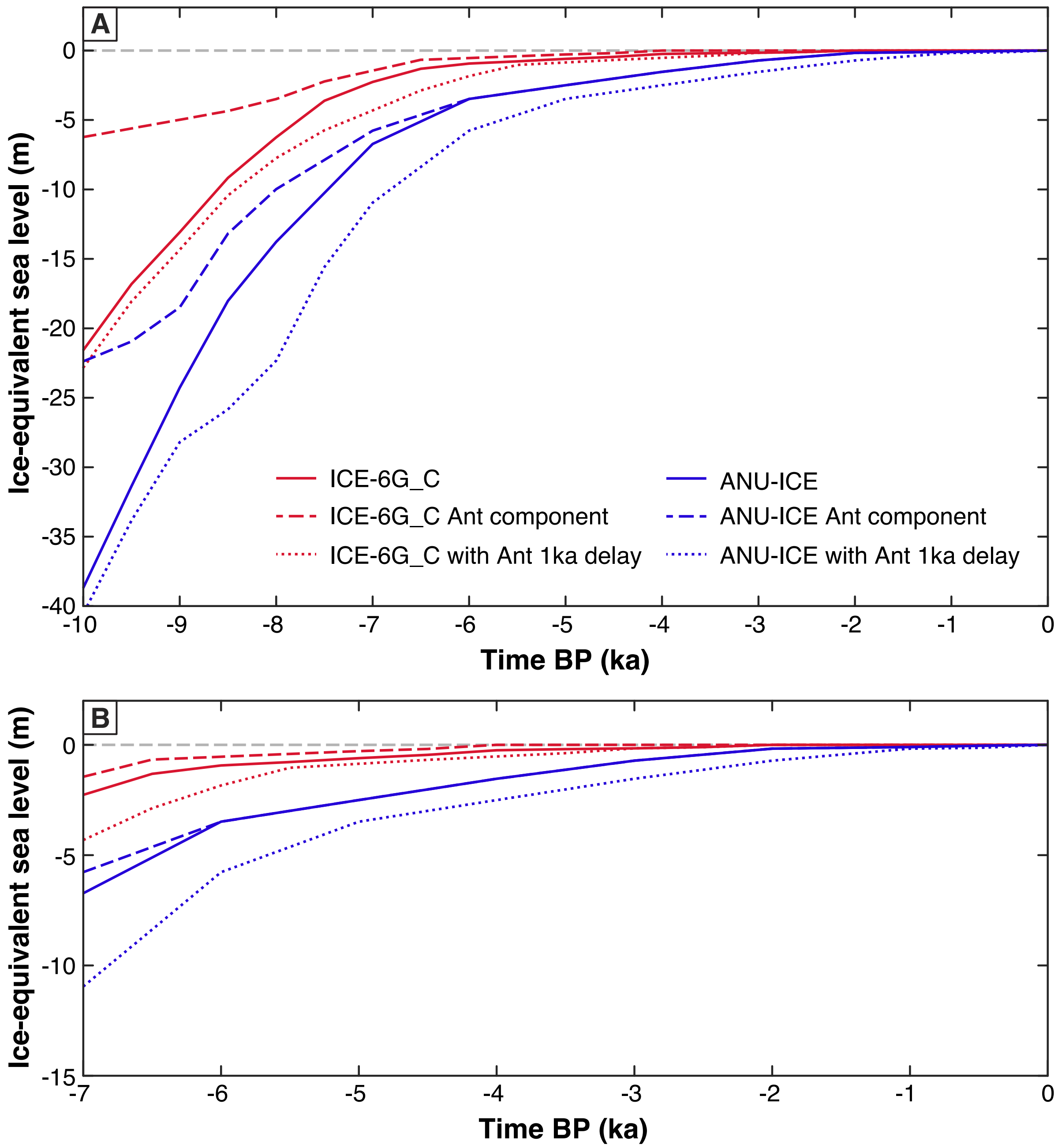

Fig. S1. Ice-equivalent sea-level (IESL, solid lines), its Antarctic component only (dashed lines) and IESL with Antarctic component deglaciation delayed for 1 ka (dotted lines) for ICE-6G_C and ANU-ICE from (A) 10 ka BP and (B) 7 ka BP till present, respectively.

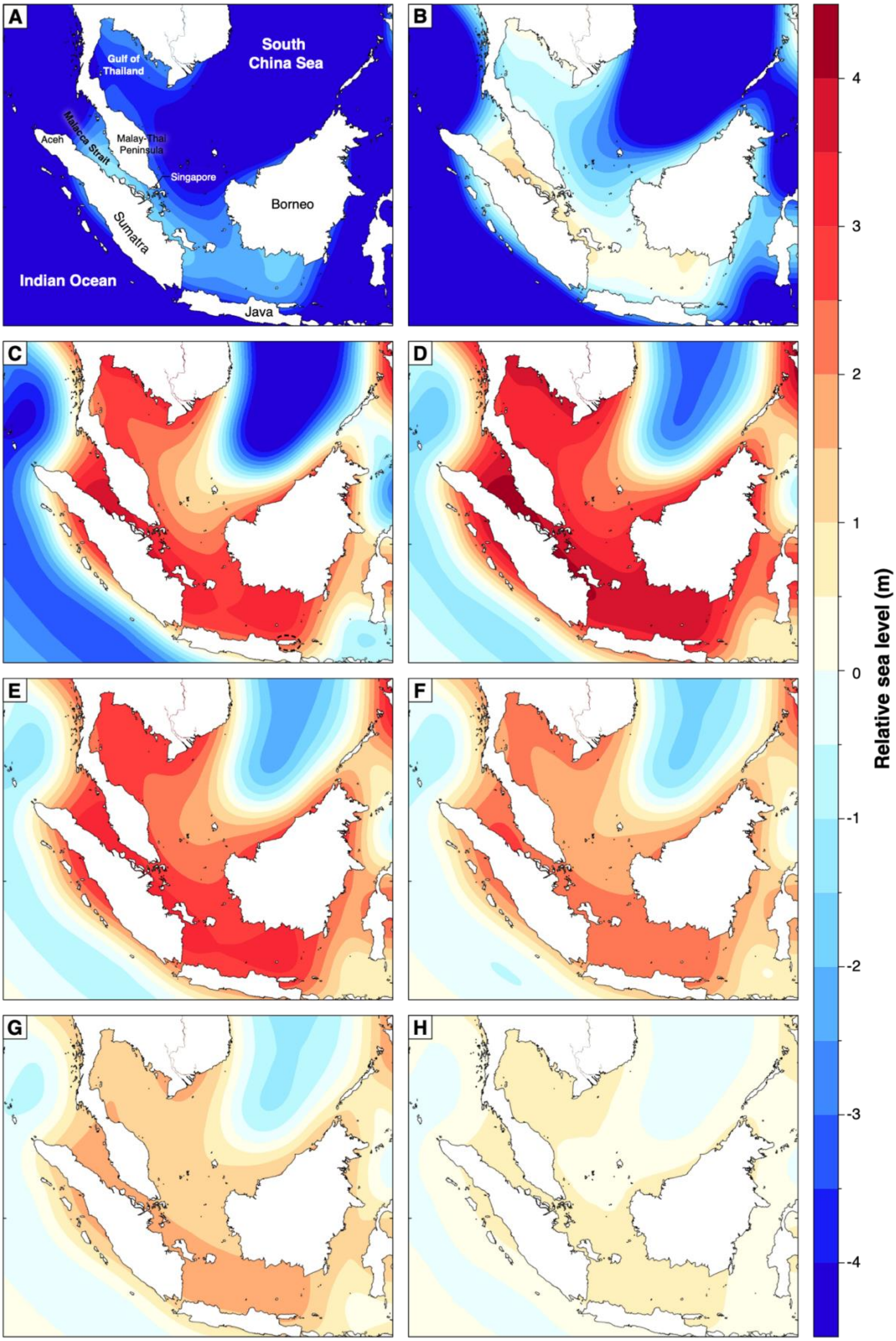
A
South China Sea
Gulf of Thailand
Malacca Strait
Aceh
Malay-Thai Peninsula
Singapore
Borneo
Sumatra
Indian Ocean
Java
B
C
D
E
F
G
H
4
3
2
1
0
-1
-2
-3
-4
Relative sea level (m)

869

Fig. S2. Relative sea-level predictions of Glacial Isostatic Adjustment model ICE-6G_C (VM5a) in Southeast Asia at (A) 9 ka BP, (B) 8.5 ka BP, (C) 7.5 ka BP, (D) 6.5 ka BP, (E) 5.5. ka BP, (F) 4.5 ka BP, (G) 3.5 ka BP, and (H) 1.5 ka BP.

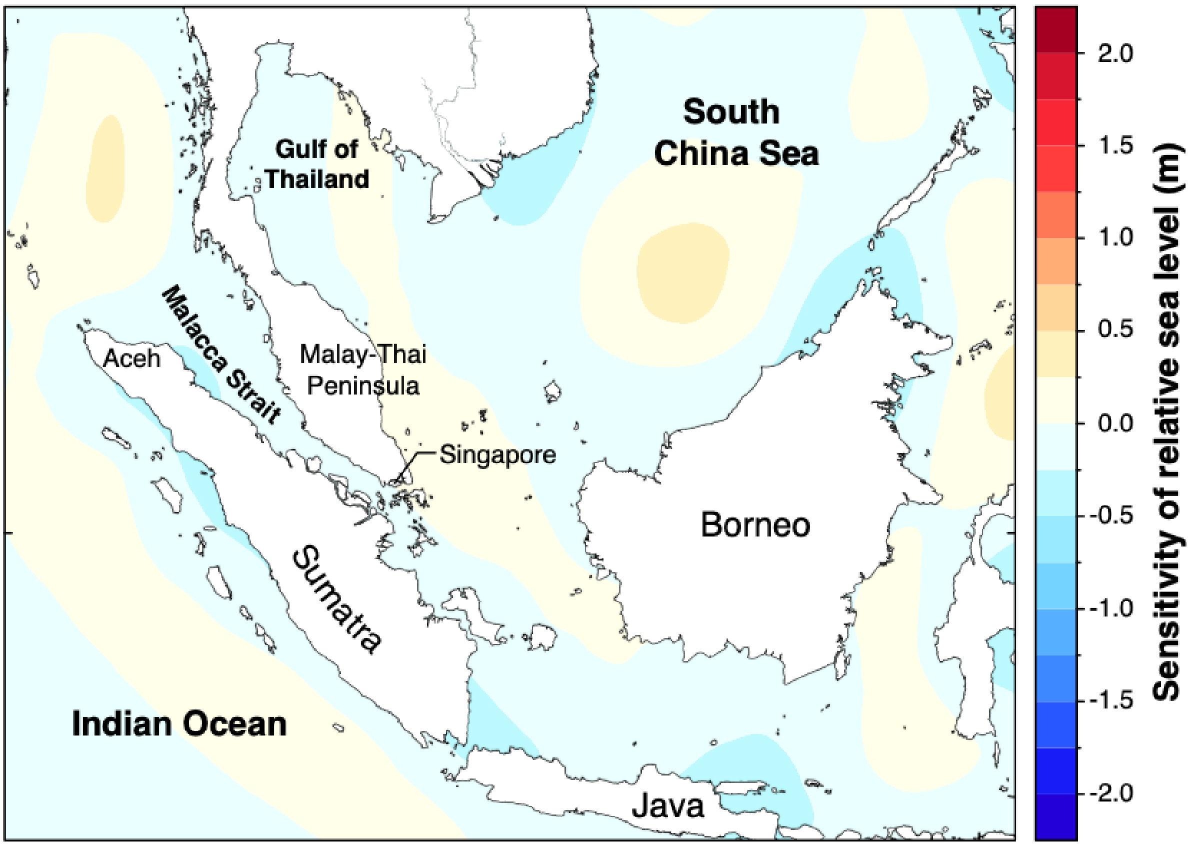

Fig. S3. Fixed with ICE-6G_C ice model, relative sea-level (RSL) sensitivity to an increase of lithospheric thickness from 60 km to 90 km at 6.5 ka BP in Southeast Asia.

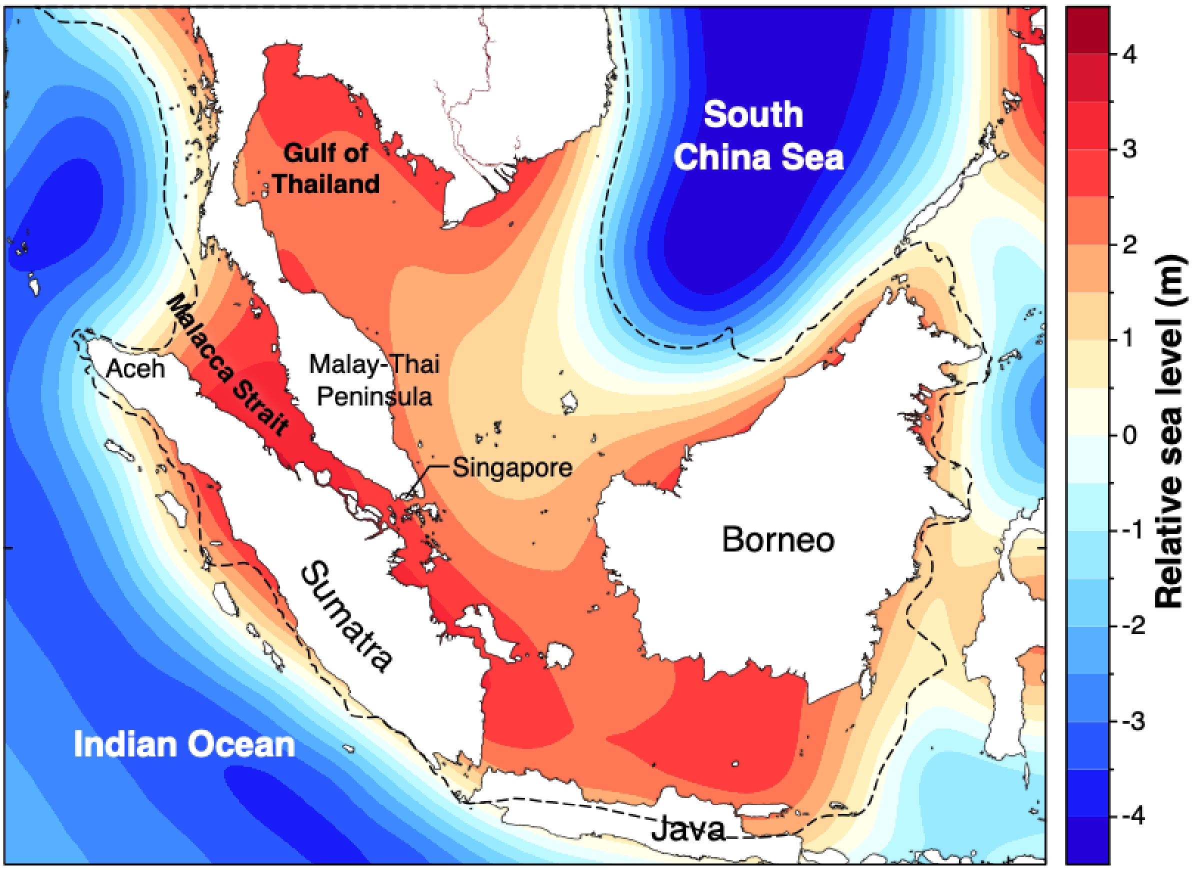

880

881 Fig. S4. Relative sea-level predictions of Glacial Isostatic Adjustment model ANU-ICE (VM5a)
882 in Southeast Asia at 6 ka BP. The black dashed line indicates the boundary of the Sundaland
883 (Hall, 2013).
884

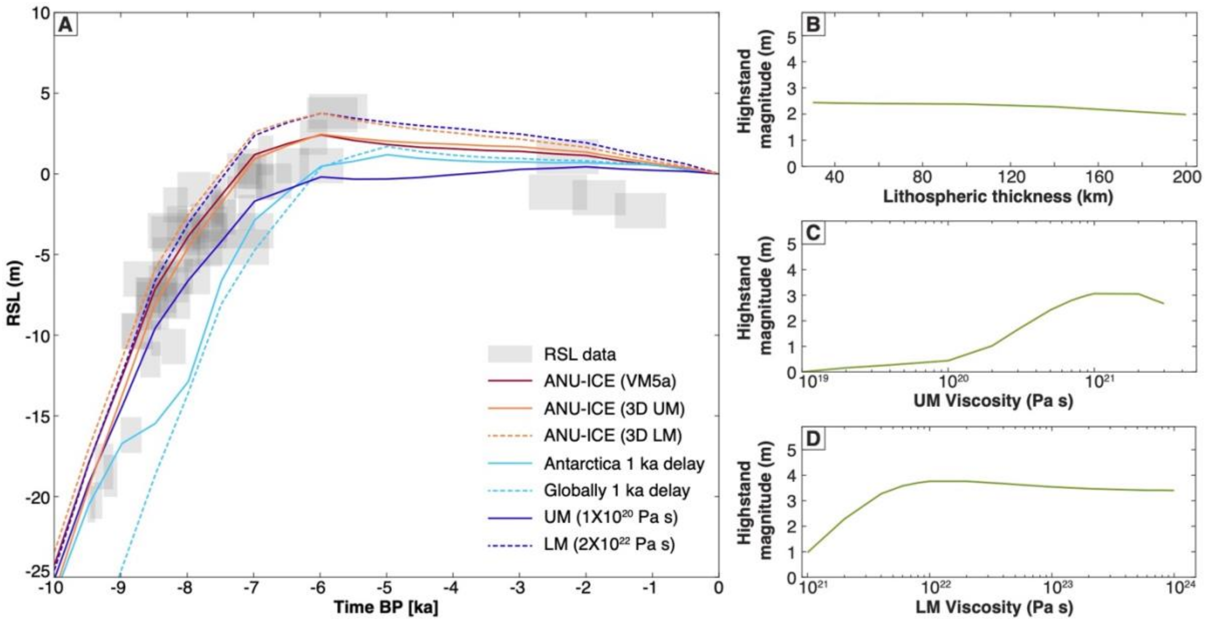

Fig. S5. (A) Reconstructed relative sea-level (RSL) data from Singapore (Chua et al., 2021) compared with RSL predictions of model ANU-ICE (VM5a) and other models that modified from ANU-ICE (VM5a). The predicted magnitude of the mid-Holocene highstand in glacial isostatic adjustment models with different (B) lithospheric thickness, (C) upper mantle (UM) viscosity, and (D) lower mantle (LM) viscosity fixed with ANU-ICE ice model.

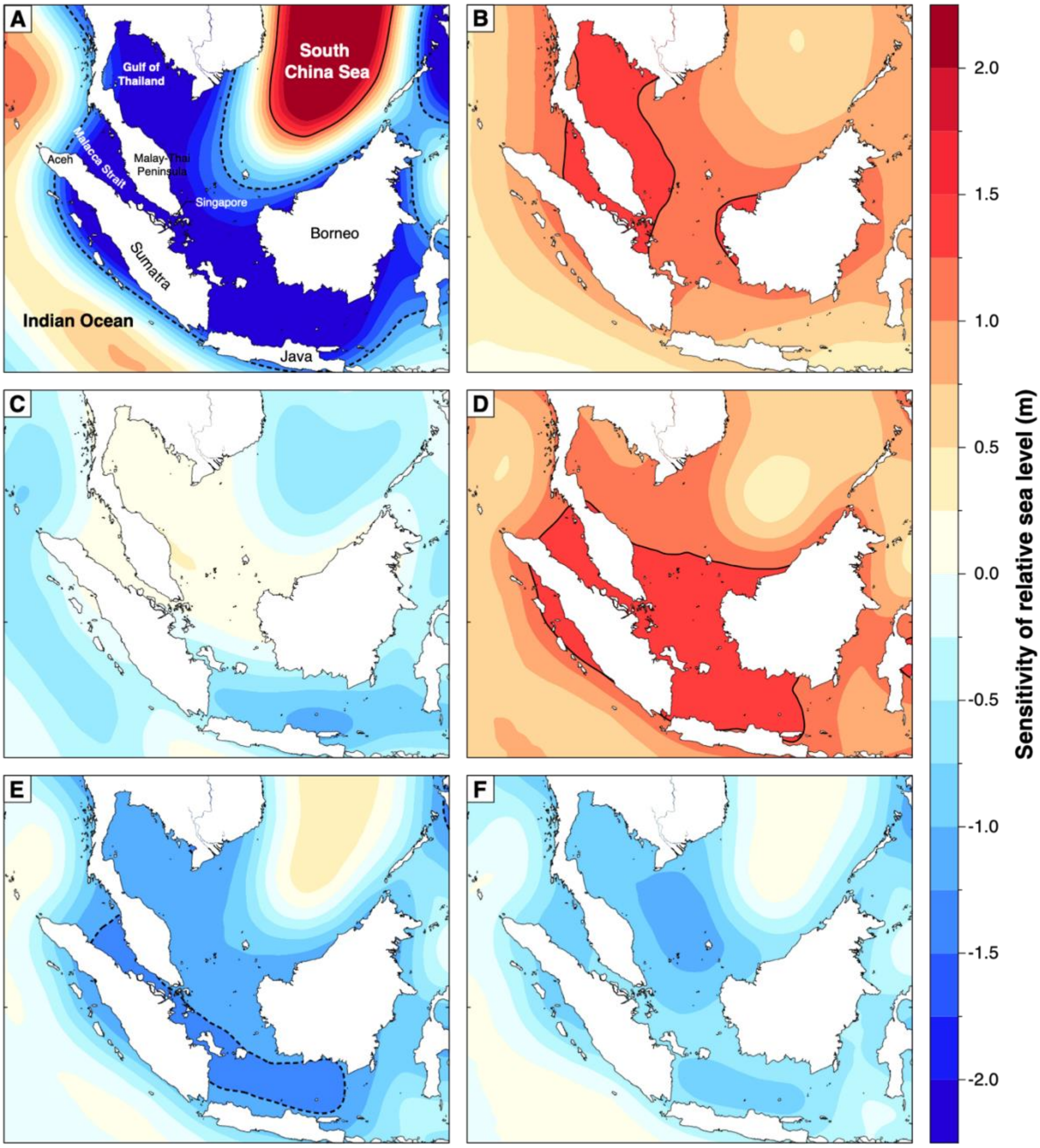

Fig. S6. Fixed with ANU-ICE ice model, relative sea-level (RSL) sensitivity to (A) 1D upper mantle viscosity (1.0 $\times 10^{20}$ Pa s), (B) 1D lower mantle viscosity (2.0 $\times 10^{22}$ Pa s), (C) 3D upper mantle viscosity, (D) 3D lower mantle viscosity at 6 ka BP in Southeast Asia. RSL peak highstand sensitivity to 1 ka delay of (E) Antarctic and (F) global ice-equivalent sea-level in Southeast Asia ($RSL_{Test}(5) - RSL_{Ref}(6)$). The black dashed and solid lines indicate the -1.25 m and 1.25 m contour lines, respectively.

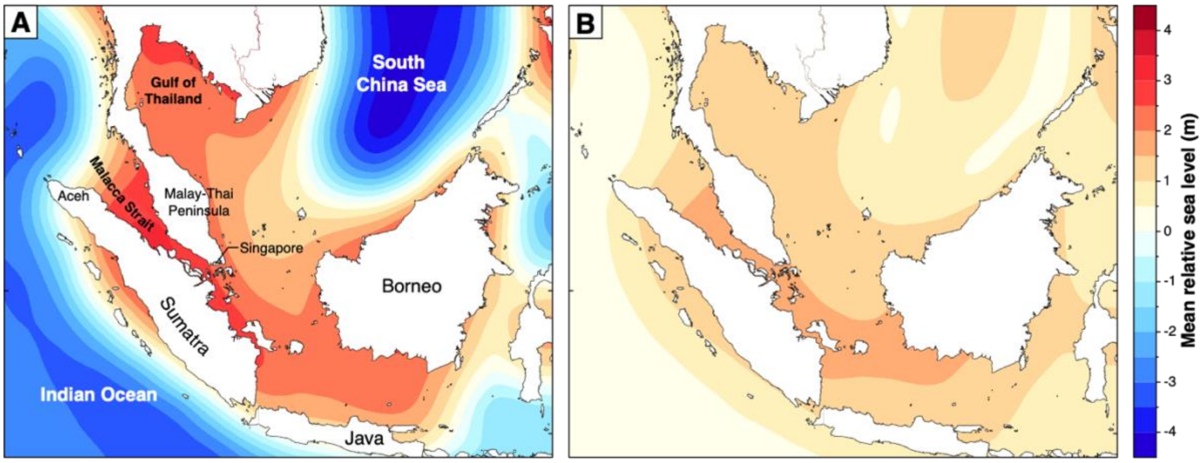

Fig. S7. Fixed with ANU-ICE ice model, (A) mean relative sea level and (B) its standard deviation at 6 ka BP in Southeast Asia calculated from the Glacial Isostatic Adjustment model ensemble consisting of 45 1D models and 2 3D models. Note that A and B share the same scale on the right.

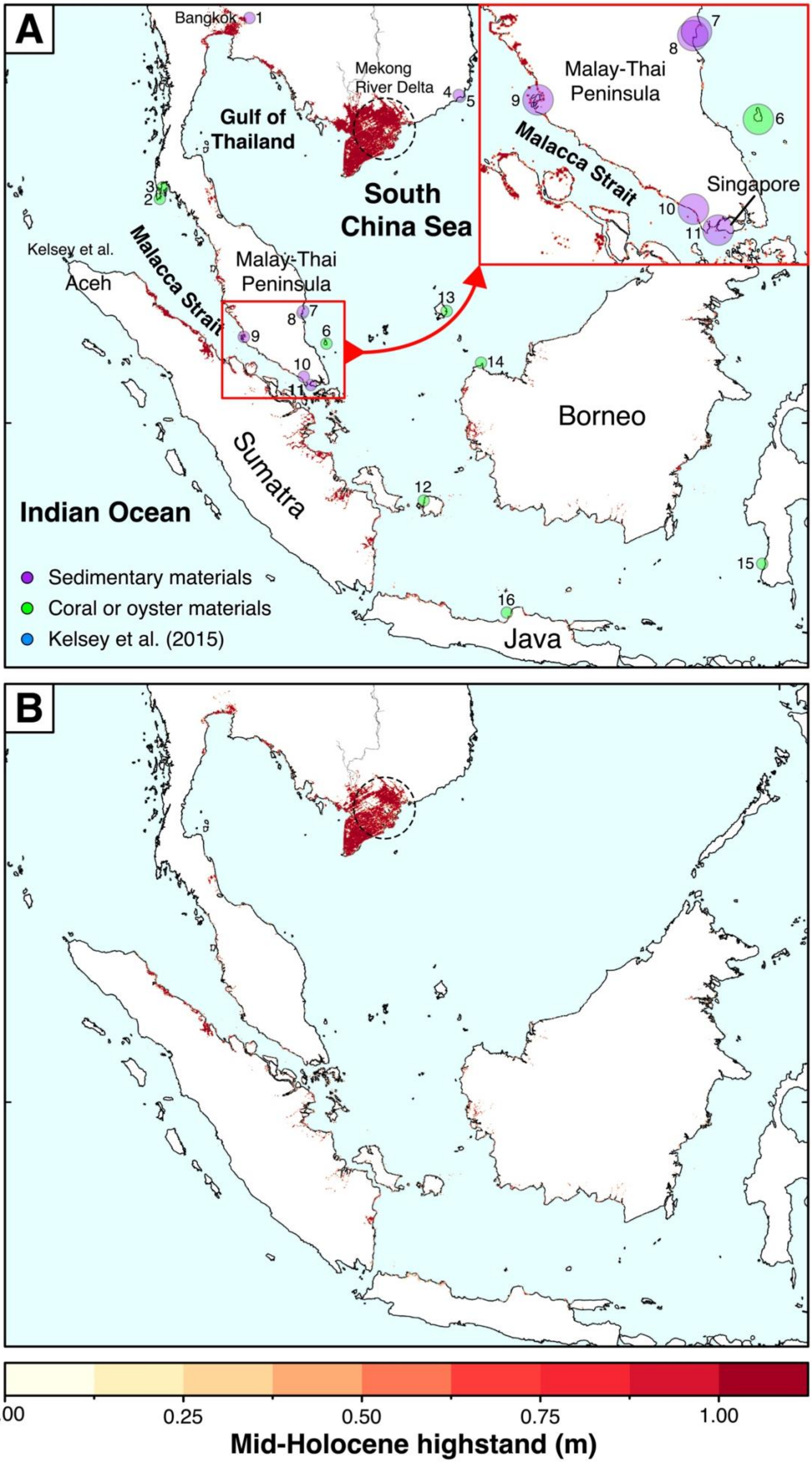
A
Bangkok
1
Mekong
River Delta
4
5
Gulf of
Thailand
South
China Sea
3
2
Kelsey et al.
Aceh
Malacca Strait
Malay-Thai
Peninsula
13
8
7
6
9
10
11
14
Borneo
Sumatra
12
Indian Ocean
Sedimentary materials
Coral or oyster materials
Kelsey et al. (2015)
15
16
Java
Malay-Thai
Peninsula
Malacca Strait
Singapore
B
0.00
0.25
0.50
0.75
1.00
Mid-Holocene highstand (m)

Fig. S8. Fixed with ANU-ICE ice model, regions that are (A) likely (67% probability) and (B) very likely (90% probability) to have the highstand record preservation considering the topography change and accommodation space across Southeast Asia. The peak highstand data summarized in Table 1 are shown in purple and green dots for sedimentary and coral or oyster materials, respectively. The sea-level reconstruction site in Aceh from Kelsey et al. (2015) showing no evidence of a highstand is shown in blue dot.

Table S1. Table of standardised indicative meanings used in the peak highstand database. RWL: reference water level; IR: indicative range; MLW: mean low water; MTL: mean tide level; MHWN: mean high water neaps; MHHW: mean higher high water; HAT: highest astronomical tide.

Indicator	Evidence	RWL	IR	References
Sea-level index points				
Mangrove sediments	Stratigraphy and/or pollen assemblage dominated by mangrove pollen (Hassan, 2001; Tam et al., 2018; Zhang et al., 2021)	$\frac{HAT+MTL}{2}$	$\frac{HAT-MTL}{2}$	Geyh et al., 1979 Somboon & Thiramongkol, 1992
Deposit from upper intertidal zone	Organic poor sands with occassional wood fragments, high bulk density (generally > 1 g/cm3), low organic content (generally < 0.5 %) (Bird et al., 2007)	$\frac{HAT+MTL}{2}$	$\frac{HAT-MTL}{2}$	Bird et al., 2010
Fossil oyster belt	Cluster of fossil oysters (Foster, 1974; Lewis et al., 2015)	$\frac{HAT+LAT}{2}$	$\frac{HAT-LAT}{2}$	Scheffers et al., 2012 Tjia et al., 1983
Marine limiting				
Massive coral/ eroded coral microatolls	Massive fossil *Porites sp.* coral with gently domed surfaces (Hibbert et al., 2016). We used the upper limit of MHWN to allow for the possibility that the corals were growing in ponded moats (Goodwin & Harvey, 2008; Scoffin et al., 1978). This includes coral microatolls with no concentric ring features and/or diedowns preserved in cross section to confirm the microatoll morphology (Meltzner & Woodroffe, 2015; Scoffin et al., 1978).	MHWN (semidiurnal tides) MHHW (mixed tides)	< MHWN (semidiurnal tides) < MHHW (mixed tides)	Scoffin & Tissier, 1998 Mann et al., 2016 Mann et al., 2023
Beachrock	Sedimentary structures and thin-section and SEM analysis showing cementation under marine phreatic conditions (lower intertidal zone) (Michelli, 2008)	MLW	< MLW	Stattegger et al., 2013
Calcareous algal crust	Calcareous algal crust that can survive above MSL depending on exposure to wave splash(Pirazzoli & Montaggioni, 1988; Tjia et al., 1983)	MHHW	< MHHW	Tjia et al., 1983

Terrestrial limiting				
Beach ridge crest	Crest of gravelly beach ridge forms above MTL (Hesp et al., 2005; Tamura, 2012)	MTL	> MTL	Stattegger et al., 2013

917

Table S2. Table of locally surveyed indicative meanings in original studies. RWL: reference water level; IR: indicative range. For coral microatolls whose elevations were surveyed relative to living equivalents, the RWL is 0 m as the elevation itself is an estimate of RSL (Tan et al., 2023).

Indicator	**Location**	**RWL**	**IR**	**References**
Sea-level index points				
Mangrove sediments	Kelang, Malaysia	1.5 m msl	1.5 ± 0.1 m msl	Hassan, 2001
Mangrove sediments (back mangrove)	Kuantan, Malaysia	1.8 m msl	1.8 ± 0.1 m msl	Hassan, 2001
Mangrove sediments (back mangrove)	Kuantan, Malaysia	1.6 m msl	1.6 ± 0.3 m msl	Zhang et al., 2021
Coral microatoll (*Porites sp.*)	Natuna, Indonesia	0.237 m above lowest predicted tide in 2012	0. 237 ± 0.287 m above lowest predicted tide in 2012	Wan et al., 2020
Coral microatoll (*Porites sp.*)	Belitung, Indonesia	0 m – elevations are relative to living counterparts	0 ± 0.25 m	Meltzner et al., 2017
Coral microatoll (*Porites sp.*)	Sarawak, Malaysia	0 m – elevations are relative to living counterparts	0 ± 0.25 m	Majewski et al., 2018

Text S1 Determination of ΔR for data no. 12

The age of the TKUB-F05 SLIP (Meltzner et al., 2017) was modelled to use the Marine20 curve by combining the radiocarbon ages of four samples with the known age separation between them based on the annual banding of the coral. The OxCal code used to determine the ΔR was adapted from Meltzner et al. (2017) as follows:

```
Plot( "TKUB")
 {
        Curve("Marine20","marine20.14c");
        Delta_R(-64,70);
               Sequence( "TKUB-F05")
               {
                      Combine()
                      {
                       R_Date("TKUB-F05-CC-D2",6392,27);
                       Gap(51);
                       R_Date("TKUB-F05-CC-D1",6419,27);
                       Gap(50);
                       R_Date("TKUB-F05-CC-A2",6361,27);
                       Gap(48);
                       R_Date("TKUB-F05-CC-A1",6389,28);
                       Gap(47);
                       Date("highest diedown TKUB F05");
                };
        };
 };
```

Note: the ΔR prior of -64 ± 70 is from Southon et al., 2002 for Marine20, obtained from the Marine20 ΔR database (Reimer & Reimer, 2001).

References

Bird, M. I., Austin, W. E. N., Wurster, C. M., Fifield, L. K., Mojtahid, M., & Sargeant, C. (2010). Punctuated eustatic sea-level rise in the early mid-Holocene. Geology, 38(9), 803–806. https://doi.org/10.1130/G31066.1

Bird, M. I., Fifield, L. K., Teh, T. S., Chang, C. H., Shirlaw, N., & Lambeck, K. (2007). An inflection in the rate of early mid-Holocene eustatic sea-level rise: A new sea-level curve from Singapore. Estuarine, Coastal and Shelf Science, 71(3–4), 523–536. https://doi.org/10.1016/j.ecss.2006.07.004

Chua, S., Switzer, A. D., Li, T., Chen, H., Christie, M., Shaw, T. A., Khan, N. S., Bird, M. I., & Horton, B. P. (2021). A new Holocene sea-level record for Singapore. The Holocene, 31(9), 1376–1390.

Foster, B. A. (1974). The Barnacles of Fiji, with Observations on the Ecology of Barnacles on Tropical Shores. Pacific Science, 28(1), 35–56.

Geyh, M. A., Streif, H., & Kudrass, H.-R. (1979). Sea-level changes during the late Pleistocene and Holocene in the Strait of Malacca. Nature, 278(5703), 441–443. https://doi.org/10.1038/278441a0

Goodwin, I. D., & Harvey, N. (2008). Subtropical sea-level history from coral microatolls in the Southern Cook Islands, since 300 AD. Marine Geology, 253(1–2), 14–25. https://doi.org/10.1016/j.margeo.2008.04.012

Hall, R. (2013). The palaeogeography of Sundaland and Wallacea since the Late Jurassic. *Journal of Limnology*, *72*.

Hassan, K. bin. (2001). Holocene sea level changes in Kelang and Kuantan, Peninsular Malaysia [Doctoral, Durham University]. http://etheses.dur.ac.uk/3786/

Hesp, P. A., Dillenburg, S. R., Barboza, E. G., Tomazelli, L. J., Ayup-Zouain, R. N., Esteves, L. S., Gruber, N. L. S., Toldo-Jr., E. E., Tabajara, L. L. C. D. A., & Clerot, L. C. P. (2005). Beach ridges, foredunes or transgressive dunefields? Definitions and an examination of the Torres to Tramandaí barrier system, Southern Brazil. Anais Da Academia Brasileira de Ciências, 77(3), 493–508. https://doi.org/10.1590/S0001-37652005000300010

Hibbert, F. D., Rohling, E. J., Dutton, A., Williams, F. H., Chutcharavan, P. M., Zhao, C., & Tamisiea, M. E. (2016). Coral indicators of past sea-level change: A global repository of

U-series dated benchmarks. Quaternary Science Reviews, 145, 1–56. https://doi.org/10.1016/j.quascirev.2016.04.019

Kelsey, H. M., Engelhart, S. E., Pilarczyk, J. E., Horton, B. P., Rubin, C. M., Daryono, M. R., Ismail, N., Hawkes, A. D., Bernhardt, C. E., & Cahill, N. (2015). Accommodation space, relative sea level, and the archiving of paleo-earthquakes along subduction zones. *Geology*, *43*(8), 675–678.

Lewis, S. E., Wüst, R. A. J., Webster, J. M., Collins, J., Wright, S. A., & Jacobsen, G. (2015). Rapid relative sea-level fall along north-eastern Australia between 1200 and 800cal.yrBP: An appraisal of the oyster evidence. Marine Geology, 370, 20–30. https://doi.org/10.1016/j.margeo.2015.09.014

Majewski, J. M., Switzer, A. D., Meltzner, A. J., Parham, P. R., Horton, B. P., Bradley, S. L., Pile, J., Chiang, H.-W., Wang, X., Ng, C. T., Tanzil, J., Müller, M., & Mujahid, A. (2018). Holocene relative sea-level records from coral microatolls in Western Borneo, South China Sea. The Holocene, 28(9), 1431–1442. https://doi.org/10.1177/0959683618777061

Meltzner, A. J., Switzer, A. D., Horton, B. P., Ashe, E., Qiu, Q., Hill, D. F., Bradley, S. L., Kopp, R. E., Hill, E. M., Majewski, J. M., Natawidjaja, D. H., & Suwargadi, B. W. (2017). Half-metre sea-level fluctuations on centennial timescales from mid-Holocene corals of Southeast Asia. Nature Communications, 8(1), 14387. https://doi.org/10.1038/ncomms14387

Meltzner, A. J., & Woodroffe, C. D. (2015). Coral microatolls. In Handbook of Sea-Level Research (pp. 125–145). John Wiley & Sons, Ltd. https://doi.org/10.1002/9781118452547.ch8

Michelli, M. (2008). Sea-level changes evolution and paleoceanography of coastal waters in SE-Vietnam since the mid-Holocene. https://macau.uni-kiel.de/receive/diss_mods_00003284

Pirazzoli, P. A., & Montaggioni, L. F. (1988). Holocene sea-level changes in French Polynesia. Palaeogeography, Palaeoclimatology, Palaeoecology, 68(2–4), 153–175. https://doi.org/10.1016/0031-0182(88)90037-5

Reimer, P. J., & Reimer, R. W. (2001). A marine reservoir correction database and on-line interface. Radiocarbon, 43(2A), 461–463.

Scheffers, A., Brill, D., Kelletat, D., Brückner, H., Scheffers, S., & Fox, K. (2012). Holocene sea levels along the Andaman Sea coast of Thailand. The Holocene, 22(10), 1169–1180. https://doi.org/10.1177/0959683612441803

Scoffin, T. P., Stoddart, D. R., & Rosen, B. R. (1978). The Nature and Significance of Microatolls. Philosophical Transactions of the Royal Society of London, 284(999), 99–122. https://doi.org/10.1098/rstb.1978.0055

Scoffin, T. P., & Tissier, M. D. A. L. (1998). Late Holocene sea level and reef-flat progradation, Phuket, South Thailand. Coral Reefs, 17(3), 273–276. https://doi.org/10.1007/s003380050128

Somboon, J. R. P., & Thiramongkol, N. (1992). Holocene highstand shoreline of the Chao Phraya delta, Thailand. Journal of Southeast Asian Earth Sciences, 7(1), 53–60. https://doi.org/10.1016/0743-9547(92)90014-3

Southon, J., Kashgarian, M., Fontugne, M., Metivier, B., & Yim, W. W.-S. (2002). Marine Reservoir Corrections for the Indian Ocean and Southeast Asia. Radiocarbon, 44(1), 167–180. https://doi.org/10.1017/S0033822200064778

Stattegger, K., Tjallingii, R., Saito, Y., Michelli, M., Trung Thanh, N., & Wetzel, A. (2013). Mid to late Holocene sea-level reconstruction of Southeast Vietnam using beachrock and beach-ridge deposits. Global and Planetary Change, 110, 214–222. https://doi.org/10.1016/j.gloplacha.2013.08.014

Tam, C.-Y., Zong, Y., Hassan, K. bin, Ismal, H. bin, Jamil, H. binti, Xiong, H., Wu, P., Sun, Y., Huang, G., & Zheng, Z. (2018). A below-the-present late Holocene relative sea level and the glacial isostatic adjustment during the Holocene in the Malay Peninsula. Quaternary Science Reviews, 201, 206–222. https://doi.org/10.1016/j.quascirev.2018.10.009

Tamura, T. (2012). Beach ridges and prograded beach deposits as palaeoenvironment records. Earth-Science Reviews, 114(3–4), 279–297. https://doi.org/10.1016/j.earscirev.2012.06.004

Tjia, H. D., Fujii, S., & Kigoshi, K. (1983). Holocene shorelines of Tioman island in the south China sea.

Wan, J. X. W., Meltzner, A. J., Switzer, A. D., Lin, K., Wang, X., Bradley, S. L., Natawidjaja, D. H., Suwargadi, B. W., & Horton, B. P. (2020). Relative Sea-level stability and the radiocarbon marine reservoir correction at Natuna Island, Indonesia, since 6400 yr BP.

Marine Geology, 106342. https://doi.org/10.1016/j.margeo.2020.106342

Zhang, Y., Zong, Y., Xiong, H., Li, T., Fu, S., Huang, G., & Zheng, Z. (2021). The middle-to-late Holocene relative sea-level history, highstand and levering effect on the east coast of Malay Peninsula. Global and Planetary Change, 196, 103369. https://doi.org/10.1016/j.gloplacha.2020.103369